

Resonator Circuits for factoring high-dimensional vectors

Spencer J. Kent*

E. Paxon Frady*

Friedrich T. Sommer

Bruno A. Olshausen

Redwood Center for Theoretical Neuroscience
University of California, Berkeley
Berkeley, CA 94702
spencer.kent@eecs.berkeley.edu

*equal contribution

Abstract

We describe a type of neural network, called a Resonator Circuit, that factors high-dimensional vectors. Given a composite vector formed by the Hadamard product of several other vectors drawn from a discrete set, a Resonator Circuit can efficiently decompose the composite into these factors. This paper focuses on the case of “bipolar” vectors whose elements are ± 1 and characterizes the solution quality, stability properties, and speed of Resonator Circuits in comparison to several benchmark optimization methods including Alternating Least Squares, Iterative Soft Thresholding, and Multiplicative Weights. We find that Resonator Circuits substantially outperform these alternative methods by leveraging a combination of powerful nonlinear dynamics and “searching in superposition”, by which we mean that estimates of the correct solution are, at any given time, formed from a weighted superposition of all possible solutions. The considered alternative methods also search in superposition, but the dynamics of Resonator Circuits allow them to strike a more natural balance between exploring the solution space and exploiting local information to drive the network toward probable solutions. Resonator Circuits can be conceptualized as a set of interconnected Hopfield Networks, and this leads to some interesting analysis. In particular, while a Hopfield Network descends an energy function and is guaranteed to converge, a Resonator Circuit is not. However, there exists a high-fidelity regime where Resonator Circuits almost always do converge, and they can solve the factorization problem extremely well. As factorization is central to many aspects of perception and cognition, we believe that Resonator Circuits may bring us a step closer to understanding how this computationally difficult problem is efficiently solved by neural circuits in brains.

1 Introduction

One explanation for the brain’s ability to apply learned knowledge in seemingly novel contexts is that it is effective at decomposing complex patterns into ones that are simpler, more fundamental, and that can be recombined in new ways to explain situations never before encountered. That this is a fundamental property of perception and cognition has been pointed out by researchers for some time (see, for instance, Rosenblatt (1962), Barrow and Tenenbaum (1978), Kersten et al. (2004), and Mumford and Desolneux (2010)). When the combination of atomic patterns is via an operation which multiplies them together to generate a composite pattern, we can call the inverse of this process – the task of decomposing the composite pattern into its constituent atoms – factorization. Factorization problems are pervasive in perception, and in order to illustrate their fundamental and diverse nature, we will highlight a few examples of prior work that has grappled with factorization in visual scenes – this paper introduces a new algorithmic and representational tool that may be useful in revisiting some of these problems.

The signal measured by an optical sensor includes the *conjunction* of many different factors. For instance, luminance at a point on the sensor is a function of physical properties in the scene, such as the reflectance and orientation of object surfaces, as well as the direction and intensity of incident illumination. Barrow and Tenenbaum (1978) hypothesized that specific physical properties might be effectively represented in a series of ‘intrinsic images’, one each for object range, surface reflectance, surface orientation, and incident illumination. Among the many follow-on works, we highlight Adelson and Pentland (1996), which took this idea, specifically the factorization of measured luminance into reflectance and incident illumination, and put it on the firmer conceptual footing of Bayesian statistical inference. At another level of abstraction, one can consider the separation of visual object features defined in some canonical object-based reference frame from the pose of objects in a larger scene. Robust object recognition depends on the ability to separate these two factors. Hinton (1981) and Olshausen et al. (1993) both addressed the problem of inferring and separately representing visual object features from object pose, with a focus on both learning and neural mechanisms by which this computation might be carried out in brains. Related to this problem in static scenes is the factorization of *dynamic* scenes into object features (also called object ‘form’) and object motion. Cadieu and Olshausen (2012) presented a hierarchical, probabilistic generative model for learning a factorization of object form and motion from natural movies. Within the Computer Vision community, the intrinsic images perspective remains dominant, with many of the more recent attempts relying on deep neural network methods. Unfortunately, these approaches are often brittle, or inefficient, or both. Uncovering factors of variation in rich three-dimensional scenes is still an open problem.

One promising strategy for solving this kind of problem is to learn a mapping into some latent space that makes factorization more tractable for an iterative algorithm such as the one we propose in this work. Our focus for now is on how to solve factorization problems in a *latent space of high-dimensional vectors*, which are assumed to represent certain structures in the original signal space, and we propose a highly efficient algorithm for doing this. The objective of this paper is therefore to establish the theoretical underpinnings of this new approach – future work will be needed to develop applications to specific percept factorization problems. Early work along these lines (Kent and Olshausen, 2017; Frady et al., 2018a)

leverages feedforward neural networks and random projections to generate high-dimensional vector representations of scenes, which can then be factored by Resonator Circuits.

Our main motivation for focusing on structure embedded in a latent space of high-dimensional vectors comes from a *family of theories* for cognitive representation called Vector Symbolic Algebras. This framework encodes concepts, be they visual scene concepts or language concepts etc., as high-dimensional vectors and defines an algebra over these vectors that can capture the structures necessary for high level cognitive processing, in particular sequences, hierarchy, and *binding/multiplication*. Inverting the binding operation of Vector Symbolic Algebras involves computing a factorization, and it was in this context that we first encountered the problem studied in this paper.

Building on ideas from Smolensky (Smolensky, 1990), Hinton (Hinton, 1990), and Touretzky (Touretzky, 1990), the first Vector Symbolic Algebra (VSA) was proposed by Plate in 1991 (Plate, 1991, 1995, 2003) under the name Holographic Reduced Representations. It underpins much of the power displayed by modern models under different names, for instance the Semantic Pointer Architecture (Eliasmith et al., 2012) and Holographic Embeddings of knowledge graphs (Nickel et al., 2016). Gayler’s Vector Symbolic Architecture (Gayler, 1998, 2004) and Kanerva’s Binary Spatter Codes (Kanerva, 1996, 2009) are also Vector Symbolic Algebras, which happen to operate with two-state vectors ($\{-1, 1\}^N$ or $\{0, 1\}^N$), and make particular use of element-wise vector multiplication to ‘bind’ factors together. We call vectors drawn from $\{-1, 1\}^N$ ‘bipolar’, and the multiplication operation between bipolar vectors is the Hadamard Product $(\mathbf{x} \odot \mathbf{y})_i = x_i y_i$. This will be our focus for the rest of the paper.

There are a number of recent works establishing the representational power of Gayler and Kanerva’s models, and we highlight three of them here. Complex relations, such as multi-argument predicates, are necessary to solve reasoning tasks like Raven’s Progressive Matrices (Raven et al., 2003). Emruli et al. (2013) showed how these relations can be represented with VSAs, using the vector algebra framework to compute solutions to these challenging problems. This work was built on earlier ideas about computing *analogies* using the VSA framework (Kanerva, 1998). A completely different application of VSAs was shown by Joshi et al. (2016), who leveraged the vector operations specified by Vector Symbolic Algebras (Multiply, Add, and Permute) to generate novel vector encodings of n-gram structure in natural language and applied this encoding to a 21-class language identification problem. Their solution, which produced high-accuracy language classifications, was very efficient and produced geometric structure among the vectors reflecting known linguistic relationships between the languages. Another recent application of Vector Symbolic Algebras is in the encoding and classification of EEG, EMG, and ECoG biosignals. Rahimi et al. (2018) surveyed recent work on this topic and proposed a highly efficient and simple processor designed for these workloads.

The applications of Vector Symbolic Algebras are broad and exciting, although more theoretical and implementation work remains for them to reach their full potential. In particular, the result of computation in VSAs is often a *composite* vector that must be decomposed in order to decode what it actually represents (for instance, a particular n-gram). This commonly involves solving a factorization problem. Until now, there has been no *efficient* way to factor the composite vectors, representing a major limitation of these models. Our algorithm, called Resonator Circuits, can efficiently solve this factorization problem and makes the use of Vector Symbolic Architecture significantly more practical.

We now give a concrete example of the factorization problem before formalizing the general case in Section 2. Suppose that a visual scene containing a single object is generated by three factors – object shape, reflectance, and pose – each of which is represented by N -dimensional bipolar vectors \mathbf{x} , \mathbf{y} , and \mathbf{z} , respectively. For now we sidestep the issue of how to get from pixels to these latent bipolar vectors, but as mentioned above please see Kent and Olshausen (2017), as well as Frady et al. (2018b), for some ideas along these lines. Assume there are ten possible shapes, six possible reflectances, and twenty-five possible poses – we write these possibilities as

$$\begin{aligned}\mathbb{X} &:= \{\mathbf{x}_1, \mathbf{x}_2, \dots, \mathbf{x}_{10}\} \\ \mathbb{Y} &:= \{\mathbf{y}_1, \mathbf{y}_2, \dots, \mathbf{y}_6\} \\ \mathbb{Z} &:= \{\mathbf{z}_1, \mathbf{z}_2, \dots, \mathbf{z}_{25}\}\end{aligned}$$

The set \mathbb{X} contains all the possible shapes, \mathbb{Y} contains all the possible reflectances, and \mathbb{Z} contains all the possible poses. In this latent space, the generative model for data \mathbf{c} is the Hadamard product of three vectors, one from each of these sets. For instance, in a particular scene we might have

$$\mathbf{c} = \mathbf{x}_3 \odot \mathbf{y}_5 \odot \mathbf{z}_{17}$$

which contains the 3rd shape, the 5th reflectance, and the 17th pose. The structure of this dataset is in some sense quite simple – there are only $10 + 6 + 25 = 41$ sources of variation. Yet, these 41 sources generate $10 \times 6 \times 25 = 1500$ possible values for \mathbf{c} . The generative model may be simple, but the task of *inference* is more challenging – given only \mathbf{c} and the sets of possible vectors \mathbb{X} , \mathbb{Y} , and \mathbb{Z} , we desire a method for determining the correct factorization $\{\mathbf{x}_3, \mathbf{y}_5, \mathbf{z}_{17}\}$ without having to search over too many of the possible factorizations.

Resonator Circuits do this by leveraging simple and powerful nonlinear dynamics as well as “search in superposition”, a notion that we make precise in the next section. There are in fact many ways to search in superposition, and we introduce a number of them in Section 2 as a way to build up to our model and to gain some deeper understanding of the problem. A Resonator Circuit is defined by equations (15) and (18), each representing two separate variants of the algorithm/network, and is named for the way in which correct factorizations seem to ‘resonate’ out of what is initially an uninformative circuit state. The size of the factorization problem that can be reliably solved, as well as the speed with which solutions are found, will characterize the performance of all the approaches we introduce – in these terms, Resonator Circuits are by far the most effective. Our main results are:

1. A characterization of solution stability compared to Hopfield Networks (Section 4.1).
2. The definition of “operational capacity” for a factorization algorithm and comparison of *eight* different algorithms on the basis of operational capacity (Section 4.2).
3. The discovery of a scaling law that relates the operational capacity of Resonator Circuits to various parameters of the factorization problem (also Section 4.2).
4. A theory for *why* Resonator Circuits perform well on this problem (Section 4.3).

We conclude with some discussion and future directions in Section 5.

2 Statement of the problem

We formalize the factorization problem in the following way: $\mathbb{X}_1, \mathbb{X}_2, \dots, \mathbb{X}_F$ are sets of vectors called ‘codebooks’. The f th codebook contains M_f ‘codevectors’ $\mathbf{x}_1^{(f)}, \mathbf{x}_2^{(f)}, \dots, \mathbf{x}_{M_f}^{(f)}$

$$\mathbb{X}_f := \{\mathbf{x}_1^{(f)}, \mathbf{x}_2^{(f)}, \dots, \mathbf{x}_{M_f}^{(f)}\} \quad \forall f = 1, 2, \dots, F$$

and these vectors all live in $\{-1, 1\}^N$. Composite vector \mathbf{c} is generated by computing the Hadamard product of F vectors, one drawn from each of the codebooks $\mathbb{X}_1, \mathbb{X}_2, \dots, \mathbb{X}_F$.

$$\begin{aligned} \mathbf{c} &= \mathbf{x}_\star^{(1)} \odot \mathbf{x}_\star^{(2)} \odot \dots \odot \mathbf{x}_\star^{(F)} \\ \mathbf{x}_\star^{(1)} &\in \mathbb{X}_1, \mathbf{x}_\star^{(2)} \in \mathbb{X}_2, \dots, \mathbf{x}_\star^{(F)} \in \mathbb{X}_F \end{aligned}$$

The factorization problem we wish to study is

$$\begin{aligned} \text{given} \quad & \mathbf{c}, \mathbb{X}_1, \mathbb{X}_2, \dots, \mathbb{X}_F \\ \text{find} \quad & \mathbf{x}_\star^{(1)} \in \mathbb{X}_1, \mathbf{x}_\star^{(2)} \in \mathbb{X}_2, \dots, \mathbf{x}_\star^{(F)} \in \mathbb{X}_F \\ \text{such that} \quad & \mathbf{c} = \mathbf{x}_\star^{(1)} \odot \mathbf{x}_\star^{(2)} \odot \dots \odot \mathbf{x}_\star^{(F)} \end{aligned} \tag{1}$$

In our example from the introduction section, $F = 3$ with $M_1 = 10$, $M_2 = 6$, and $M_3 = 25$. Our assumption is generally that there are no repeated codevectors, so that the factorization of \mathbf{c} into F codevectors, one from each codebook, is unique. Then, the total number of composite vectors that can be generated by the codebooks is M :

$$M := \prod_{f=1}^F M_f$$

The problem involves searching among M possible factorizations to find the one that generates \mathbf{c} . We will refer to M as the search space size, and at some level it captures the difficulty of the problem. The problem size is also affected by N , the dimensionality of each vector.

Suppose we were to solve (1) using a brute force strategy. We might form all possible composite vectors from the sets $\mathbb{X}_1, \mathbb{X}_2, \dots, \mathbb{X}_F$, one at a time, until we generate the vector \mathbf{c} , which would indicate the appropriate factorization. Assuming no additional information is available, the number of trials taken to find the correct factorization is a uniform random variable $K \sim \mathcal{U}\{1, M\}$ and thus $\mathbf{E}[K] = \frac{M+1}{2}$. If instead we could easily store all of the composite vectors ahead of time, we could compare them to any new composite vector via a single matrix-vector inner product, which, assuming the factorization is unique, will yield a value of N for the correct factorization and values strictly less than N for all other factorizations. The matrix containing all possible composite vectors requires MN bits to store. The core issue is that M scales *very* poorly with the number of factors and number of possible codevectors to be entertained. If $F = 4$ (4 factors) and $M_f = 100 \forall f$ (100 possible codevectors for each factor), then $M = 100,000,000$. In the context of Vector Symbolic Algebras, it is common to have $N = 10,000$. Therefore, the matrix with all possible composite vectors would require ≈ 125 GB to store. We aspire to solve problems of this size (and much larger), which are clearly out of reach for brute-force approaches. Fortunately, they are solvable using Resonator Circuits.

2.1 Factoring by search in superposition

In our problem formulation (1) the factors interact multiplicatively to form \mathbf{c} , and this lies at the heart of what makes it hard to solve. One way to attempt a solution is to produce an estimate for each factor in turn, alternating between updates to a single factor on its own, with the others held fixed. In addition, it may make sense to simulatenously entertain all of the vectors in each \mathbb{X}_f , in some proportion that reflects our current confidence in each one being part of the correct solution. We call this *searching in superposition* and it is the general approach we take throughout the paper. What we mean by ‘superposition’ is that the estimate for the f th factor, $\hat{\mathbf{x}}^{(f)}$, is given by $\hat{\mathbf{x}}^{(f)} = g(\mathbf{X}_f \mathbf{a}_f)$ where \mathbf{X}_f is a matrix with each column a vector from \mathbb{X}_f . The vector \mathbf{a}_f contains the coefficients that define a linear combination of the elements of \mathbb{X}_f , and $g(\cdot)$ is a function from \mathbb{R}^N to \mathbb{R}^N , which we will call the activation function. ‘Search’ refers to the method by which we adapt \mathbf{a}_f over time. The estimate for each factor leads to an estimate for \mathbf{c} denoted by $\hat{\mathbf{c}}$:

$$\hat{\mathbf{c}} := \hat{\mathbf{x}}^{(1)} \odot \hat{\mathbf{x}}^{(2)} \odot \dots \odot \hat{\mathbf{x}}^{(F)} = g(\mathbf{X}_1 \mathbf{a}_1) \odot g(\mathbf{X}_2 \mathbf{a}_2) \odot \dots \odot g(\mathbf{X}_F \mathbf{a}_F) \quad (2)$$

Suppose $g(\cdot)$ is the identity $g : \mathbf{x} \mapsto \mathbf{x}$. Then $\hat{\mathbf{c}}$ becomes a *multilinear* function of the coefficients $\mathbf{a}_1, \mathbf{a}_2, \dots, \mathbf{a}_F$.

$$\hat{\mathbf{c}} = \hat{\mathbf{x}}^{(1)} \odot \hat{\mathbf{x}}^{(2)} \odot \dots \odot \hat{\mathbf{x}}^{(F)} = \mathbf{X}_1 \mathbf{a}_1 \odot \mathbf{X}_2 \mathbf{a}_2 \odot \dots \odot \mathbf{X}_F \mathbf{a}_F \quad (3)$$

While this is a ‘nice’ relationship in the sense that it is linear in each of the coefficients \mathbf{a}_f separately (with the others held fixed), it is unfortunately not convex with respect to the coefficients taken all at once. We can rewrite it as a sum of M different terms, one for each of the possible factorizations of \mathbf{c} :

$$\hat{\mathbf{c}} = \sum_{m_1, m_2, \dots, m_F} \left((\mathbf{a}_1)_{m_1} (\mathbf{a}_2)_{m_2} \dots (\mathbf{a}_F)_{m_F} \right) \mathbf{x}_{m_1}^{(1)} \odot \mathbf{x}_{m_2}^{(2)} \odot \dots \odot \mathbf{x}_{m_F}^{(F)} \quad (4)$$

Where m_1 ranges from 1 to M_1 , m_2 ranges from 1 to M_2 , and so on. The term in parentheses is a scalar that weights each of the possible Hadamard products. Our estimate $\hat{\mathbf{c}}$ is, at any given time, purely a superposition of *all* the possible factorizations. Moreover, the superposition weights $\left((\mathbf{a}_1)_{m_1} (\mathbf{a}_2)_{m_2} \dots (\mathbf{a}_F)_{m_F} \right)$ can be approximately recovered from $\hat{\mathbf{c}}$ alone by computing the cosine similarity between $\hat{\mathbf{c}}$ and the vector $\mathbf{x}_{m_1}^{(1)} \odot \mathbf{x}_{m_2}^{(2)} \odot \dots \odot \mathbf{x}_{m_F}^{(F)}$. The source of ‘noise’ in this approximation is the fact that $\mathbf{x}_{m_1}^{(1)} \odot \mathbf{x}_{m_2}^{(2)} \odot \dots \odot \mathbf{x}_{m_F}^{(F)}$ will have some nonzero inner product with the other vectors in the sum. When the codevectors are uncorrelated and high-dimensional, this noise is quite small: $\hat{\mathbf{c}}$ transparently reflects the proportion with which it contains each of the possible factorizations. When $g(\cdot)$ is a nonlinear activation function, for instance the sign function $g : \mathbf{x} \mapsto \text{sgn}(\mathbf{x})$, *this property is retained*. The vector $\hat{\mathbf{c}}$ is no longer an exact superposition, but the scalar $\left((\mathbf{a}_1)_{m_1} (\mathbf{a}_2)_{m_2} \dots (\mathbf{a}_F)_{m_F} \right)$ can still be decoded from $\hat{\mathbf{c}}$ in the same way – the vector $\hat{\mathbf{c}}$ is still an approximate superposition of all the possible factorizations, with the weight for each of these determined by the coefficients \mathbf{a}_f . This property, that thresholded superpositions retain relative similarity to each of their superimposed components, is heavily relied on throughout Kanerva’s and Gayler’s work on Vector Symbolic Algebras (Kanerva, 1996; Gayler, 1998).

2.2 Search as an optimization problem

The most natural strategy to find the correct factors is to define a loss function which compares the current estimate $\hat{\mathbf{c}} := \hat{\mathbf{x}}^{(1)} \odot \hat{\mathbf{x}}^{(2)} \odot \dots \odot \hat{\mathbf{x}}^{(F)}$ with the composite that is to be factored, \mathbf{c} . One can choose a loss function and a constraint set so that the global minimizer of this loss over the constraints yields the correct solution to (1). Let the loss function be $\mathcal{L}(\mathbf{c}, \hat{\mathbf{c}})$ and the feasible set for each \mathbf{a}_f be C_f . This suggests a fairly generic optimization problem:

$$\begin{aligned} & \underset{\mathbf{a}_1, \mathbf{a}_2, \dots, \mathbf{a}_F}{\text{minimize}} && \mathcal{L}(\mathbf{c}, g(\mathbf{X}_1 \mathbf{a}_1) \odot g(\mathbf{X}_2 \mathbf{a}_2) \odot \dots \odot g(\mathbf{X}_F \mathbf{a}_F)) \\ & \text{subject to} && \mathbf{a}_1 \in C_1, \mathbf{a}_2 \in C_2, \dots, \mathbf{a}_F \in C_F \end{aligned} \quad (5)$$

the details of which may be heavily dependent on our choices for $\mathcal{L}(\cdot, \cdot)$, $g(\cdot)$, C_1, C_2, \dots, C_F , and the structure of the vectors in each codebook. Different optimization algorithms may be appropriate for this problem, depending on the particular form of (5), and we propose *six* candidate algorithms in this paper, which we refer to as the ‘‘benchmarks’’. The dynamics for each of the benchmark algorithms are compiled in Table 1, briefly reviewed in Section 2.3, and discussed at some length in the Appendix. Our algorithm, called a Resonator Circuit, does not take this approach (i.e. defining a loss function which is consistently minimized by the dynamics). Instead, it is best understood as a nonlinear dynamical system whose fixed points are likely to yield the correct factorization (by design), and whose dynamics *approximately* move the state $\hat{\mathbf{c}}$ towards \mathbf{c} .

Our notation will often include an explicit dependence on time t like so: $\hat{\mathbf{x}}_f[t] = g(\mathbf{X}_f \mathbf{a}_f[t])$. Also, we define the vector $\hat{\mathbf{o}}^{(f)}$ to be the product of the estimates for the *other* factors:

$$\hat{\mathbf{o}}^{(f)} := \hat{\mathbf{x}}^{(1)} \odot \dots \odot \hat{\mathbf{x}}^{(f-1)} \odot \hat{\mathbf{x}}^{(f+1)} \odot \dots \odot \hat{\mathbf{x}}^{(F)} \quad (6)$$

This will come up in each of the algorithms under consideration and simplify the notation in what follows. Each of the algorithms considered in this paper updates one factor at a time, with the others held fixed so, at a given time t , we will update the factors in order 1 to F , although this is a somewhat arbitrary choice. Including time dependence with $\hat{\mathbf{o}}^{(f)}$, we have

$$\hat{\mathbf{o}}^{(f)}[t] := \hat{\mathbf{x}}^{(1)}[t+1] \odot \dots \odot \hat{\mathbf{x}}^{(f-1)}[t+1] \odot \hat{\mathbf{x}}^{(f+1)}[t] \odot \dots \odot \hat{\mathbf{x}}^{(F)}[t] \quad (7)$$

which makes explicit that at the time of updating $\hat{\mathbf{x}}_f$, the factors 1 to $(f-1)$ have already been updated for this ‘iteration’ t while the factors $(f+1)$ to F have yet to be updated.

2.3 Benchmark algorithms

A common thread among all the algorithms that we introduce in this section is the fact that the function $g(\cdot)$ is the identity $g : \mathbf{x} \mapsto \mathbf{x}$, making $\hat{\mathbf{c}}$ a multilinear function of the coefficients, as we discussed above. We consider two straightforward loss functions for comparing \mathbf{c} and $\hat{\mathbf{c}}$. The first is one half the squared Euclidean norm of the error, $\mathcal{L} : \mathbf{x}, \mathbf{y} \mapsto \frac{1}{2} \|\mathbf{x} - \mathbf{y}\|_2^2$, which we will call the squared error for short, and the second is the negative inner product $\mathcal{L} : \mathbf{x}, \mathbf{y} \mapsto -\langle \mathbf{x}, \mathbf{y} \rangle$. The squared error is minimized by $\hat{\mathbf{c}} = \mathbf{c}$, which is also true for the negative inner product when $\hat{\mathbf{c}}$ is constrained to $[-1, 1]^N$. Both of these loss functions are convex, meaning that $\mathcal{L}(\mathbf{c}, \hat{\mathbf{c}})$ is a convex function of each \mathbf{a}_f separately¹. *Some* of the

¹through the composition of an affine function with a convex function

benchmark algorithms constrain \mathbf{a}_f directly, and when that is the case, our focus is on three different convex sets, namely the simplex $\Delta_{M_f} := \{\mathbf{x} \in \mathbb{R}^{M_f} \mid \sum_i x_i = 1, x_i \geq 0 \forall i\}$, the unit ℓ_1 ball $\mathcal{B}_{\|\cdot\|_1}[1] := \{\mathbf{x} \in \mathbb{R}^{M_f} \mid \|\mathbf{x}\|_1 \leq 1\}$, and the closed zero-one hypercube $[0, 1]^{M_f}$. Therefore, solving (5) with respect to each \mathbf{a}_f *separately* is a convex optimization problem. In the case of the negative inner product loss $\mathcal{L} : \mathbf{x}, \mathbf{y} \mapsto -\langle \mathbf{x}, \mathbf{y} \rangle$ and simplex constraints $C_f = \Delta_{M_f}$, it is a bonafide linear program. The correct factorization is given by $\mathbf{a}_1^*, \mathbf{a}_2^*, \dots, \mathbf{a}_F^*$ such that $\hat{\mathbf{x}}^{(f)} = \mathbf{X}_f \mathbf{a}_f^* = \mathbf{x}_*^{(f)} \forall f$, which we know to be vectors with a single entry 1 and the rest 0 – these are the standard basis vectors \mathbf{e}_i (where $(\mathbf{e}_i)_j = 1$ if $j = i$ and 0 otherwise). According to the problem statement (1), any algorithm we choose to solve the superposition search must determine initial values for $\mathbf{a}_1, \mathbf{a}_2, \dots, \mathbf{a}_F$ (which we notate as $\mathbf{a}_1[0], \mathbf{a}_2[0], \dots, \mathbf{a}_F[0]$) using only the vector \mathbf{c} and the sets \mathbb{X}_f . There is no additional information about how to set $\mathbf{a}_f[0]$. A sensible thing to do would be to set each element of $\mathbf{a}_f[0]$ to the same value so that each of the potential codevectors is equally weighted in the superposition that forms the initial estimate $\hat{\mathbf{x}}^{(f)}[0] = \mathbf{X}_f \mathbf{a}_f[0]$.

2.3.1 Alternating Least Squares

Alternating Least Squares (ALS) locally minimizes the squared error loss in a fairly straightforward way: for each factor, one at a time, it solves a least squares problem for \mathbf{a}_f and updates the current state of the estimate $\hat{\mathbf{c}}$ to reflect this new value, then moves onto the next factor and repeats. Formally, the updates given by Alternating Least Squares are:

$$\begin{aligned} \mathbf{a}_f[t+1] &= \arg \min_{\mathbf{a}_f} \frac{1}{2} \|\mathbf{c} - \hat{\mathbf{o}}^{(f)}[t] \odot \mathbf{X}_f \mathbf{a}_f[t]\|_2^2 \\ &= (\boldsymbol{\xi}^T \boldsymbol{\xi})^{-1} \boldsymbol{\xi}^T \mathbf{c} \quad | \quad \boldsymbol{\xi} := \text{diag}(\hat{\mathbf{o}}^{(f)}[t]) \mathbf{X}_f \end{aligned}$$

Alternating Least Squares is an algorithm that features prominently in the tensor decomposition literature (Kolda and Bader, 2009), but while ALS has been successful for a particular type of tensor decomposition, there are a few details which make our problem different from what is normally studied (see Appendix A). The updates in ALS are quite greedy – they exactly solve each least squares subproblem. It may make sense to more gradually modify the coefficients, a strategy that we turn to next.

2.3.2 Gradient-following algorithms

Another natural strategy for solving (5) is to make updates that incorporate the gradient of \mathcal{L} with respect to the coefficients – each of the next 5 algorithms does this in a particular way. The squared error loss is globally minimized by $\hat{\mathbf{c}} = \mathbf{c}$, so one might be tempted to start from some initial values for the coefficients and make gradient updates $\mathbf{a}_f[t+1] = \mathbf{a}_f[t] - \eta \nabla_{\mathbf{a}_f} \mathcal{L}$. In Appendix B.1 we discuss why this does not work well – the difficulty is in being able to guarantee that the loss function is *smooth* enough that gradient descent iterates with a *fixed* stepsize will converge. Instead, the algorithms we apply to the squared error loss utilize a dynamic stepsize.

The global minimizers of (5) are maximally sparse, $\|\mathbf{a}_f^*\|_0 = 1$. If one aims to minimize the squared error loss while *loosely* constrained to sparse solutions, it may make sense to solve the problem with **Iterative Soft Thesholding (ISTA)**. The dynamics for ISTA are given

by equation (9). The dynamic stepsize η can be set via backtracking line search or, as we did, by computing the Lipschitz constant of the function gradient. The only free parameter for ISTA is λ , which effectively sets the sparsity of solutions that are considered. We discuss this, as well as some context and motivation for ISTA, in Appendix C. We also considered **Fast Iterative Soft Thesholding (FISTA)**, an enhancement due to Beck and Teboulle (2009), which utilizes Nesterov’s momentum for accelerating first-order methods in order to alleviate the sometimes slow convergence of ISTA (Bredies and Lorenz, 2008). Dynamics for FISTA are given in equation (10). Another benchmark algorithm we considered was **Projected Gradient Descent** on the negative inner product loss, where updates were projected onto either the simplex or unit ℓ_1 ball (11). A detailed discussion of this approach can be found in Appendix D. **Multiplicative Weights** is an algorithm that can be applied to either loss function, although we found it worked best on the negative inner product. It very elegantly enforces a simplex constraint on \mathbf{a}_f by maintaining a set of auxilliary variables, the ‘weights’, which are used to set \mathbf{a}_f at each iteration. Both Projected Gradient Descent and Multiplicative Weights have a single hyperparameter, η , which sets the stepsize of each iteration. See equation (12) for the dynamics of Multiplicative Weights, as well as Appendix E. The final algorithm that we considered is called **Map Seeking Circuits**. Map Seeking Circuits are neural networks designed to solve invariant pattern recognition problems using the principle of superposition. Their dynamics are based on the gradient, but are different from what we have introduced so far – see equation (13) and Appendix F.

2.4 Summary of Benchmark Algorithms

The most natural way to approach vector factorization problem (1) is to cast it as a problem of optimization, centered around the minimization of a loss function $\mathcal{L}(\mathbf{c}, \hat{\mathbf{c}})$. We have proposed six algorithms falling within this framework that all utilize the principle of search in superposition (see Section 2.1) but whose dynamics vary substantially. In the Appendix we prove, or refer to results proving, that *each one of them converges for all initial conditions*. That is, given any starting coefficients $\mathbf{a}_f[0]$, their dynamics reach fixed points which are local minimizers of the loss function. The optimization problem being solved is fundamentally non-convex, so this fact alone may not tell us much about the quality of the local minima that are found in practice. In Section 4 we will establish a standard setting where we measure how likely it is that these local minima are actually *global* minima. We find that as long as M – the size of the search space – is small enough, each of these algorithms can find the global minimizers reliably. The point at which the problem becomes too large to reliably solve is what we call the operational capacity of the algorithm, and will be the main point of comparison with our model, which we introduce next. The benchmarks we have proposed are a subset of the optimization-based approaches we tried for solving the factorization problem. This included experimenting with different activation functions, different constraints, and different dynamics. The algorithms presented in this section represent the strongest benchmarks we could find.

Algorithm	Dynamics for updating factor coefficients $\mathbf{a}_f[t]$	Eq.
Alternating Least Squares	$\mathbf{a}_f[t+1] = (\boldsymbol{\xi}^T \boldsymbol{\xi})^{-1} \boldsymbol{\xi}^T \mathbf{c}$ $\boldsymbol{\xi} := \text{diag}(\hat{\mathbf{o}}^{(f)}[t]) \mathbf{X}_f$	(8)
Iterative Soft Thresholding	$\mathbf{a}_f[t+1] = \mathcal{S}[\mathbf{a}_f[t] - \eta \nabla_{\mathbf{a}_f} \mathcal{L}; \lambda \eta]$ $(\mathcal{S}[\mathbf{x}; \gamma])_i := \text{sgn}(x_i) \max(x_i - \gamma, 0)$	(9)
Fast Iterative Soft Thresholding	$\alpha_t = \frac{1 + \sqrt{1 + 4\alpha_{t-1}^2}}{2}$ $\beta_t = \frac{\alpha_{t-1} - 1}{\alpha_t}$ $\mathbf{p}_f[t+1] = \mathbf{a}_f[t] + \beta_t(\mathbf{a}_f[t] - \mathbf{a}_f[t-1])$ $\mathbf{a}_f[t+1] = \mathcal{S}[\mathbf{p}_f[t+1] - \eta \nabla_{\mathbf{p}_f} \mathcal{L}; \lambda \eta]$ $(\mathcal{S}[\mathbf{x}; \gamma])_i := \text{sgn}(x_i) \max(x_i - \gamma, 0)$	(10)
Projected Gradient Descent	$\mathbf{a}_f[t+1] = \mathcal{P}_{C_f}[\mathbf{a}_f[t] - \eta \nabla_{\mathbf{a}_f} \mathcal{L}]$ $\mathcal{P}_{C_f}[\mathbf{x}] := \arg \min_{\mathbf{z} \in C_f} \frac{1}{2} \ \mathbf{x} - \mathbf{z}\ _2^2$	(11)
Multiplicative Weights	$\mathbf{w}_f[t+1] = \mathbf{w}_f[t] \odot \left(\mathbf{1} - \frac{\eta}{\rho} \nabla_{\mathbf{a}_f} \mathcal{L} \right)$ $\mathbf{a}_f[t+1] = \frac{\mathbf{w}_f[t+1]}{\sum_i w_{fi}[t+1]}$ $\rho := \max_i (\nabla_{\mathbf{a}_f} \mathcal{L})_i $	(12)
Map Seeking Circuits	$\mathbf{a}_f[t+1] = \mathcal{T}\left(\mathbf{a}_f[t] - \eta \left(\mathbf{1} + \frac{1}{\rho} \nabla_{\mathbf{a}_f} \mathcal{L}\right); \epsilon\right)$ $\mathcal{T}(\mathbf{x}; \epsilon)_i := \begin{cases} x_i & \text{if } x_i \geq \epsilon \\ 0 & \text{otherwise} \end{cases}$ $\rho := \left \min_i (\nabla_{\mathbf{a}_f} \mathcal{L})_i \right $	(13)

Table 1: Dynamics for \mathbf{a}_f , benchmark algorithms. (see text, including Appendices, for discussion of hyperparameters η , λ , and ϵ , as well as initial conditions).

3 Resonator Circuits

The benchmark algorithms we have so far introduced generate estimates for the factors $\hat{\mathbf{x}}^{(f)}[t]$ that move through the interior of the $[-1, 1]$ hypercube. Our proposal, a neural network called a Resonator Circuit, does not. It uses the highly nonlinear activation function $g : \mathbf{x} \mapsto \text{sgn}(\mathbf{x})$, which ‘bipolarizes’ inputs to the nearest vertex of the hypercube. It also does not use additive gradient-based updates but rather alternating projections onto the linear subspace spanned by the codevectors. We know the solutions $\mathbf{x}_\star^{(f)}$ exist at vertices of the hypercube and these points are very special geometrically in the sense that in high dimensions, most of the mass of $[-1, 1]^N$ is concentrated relatively *far* from the vertices – a fact we will not prove here but that is based on standard results from the study of concentration inequalities (Boucheron et al., 2013). It may be that moving through the interior of the hypercube during the search for a factorization is unwise, and instead the search should be limited to vertices of the hypercube.

It is the combination of projections and binarization that distinguishes our approach. This is not a trivial modification to what we have already covered – adding to the gradient-based algorithms a saturating nonlinearity (either the sign function or something else) does not yield improvement in their performance, and removing the activation function in a Resonator Circuit worsens its performance – it is the *combination* of these two choices that gives our model its significant advantage in operational capacity, a metric we define and measure in Section 4.2.

3.1 Resonator Circuit with Ordinary Least Squares weights

We will first write down the dynamics for this model and then discuss various algorithmic and neural network interpretations. A Resonator Circuit with Ordinary Least Squares (OLS) weights is given by:

$$\mathbf{a}_f[t + 1] = (\mathbf{X}_f^T \mathbf{X}_f)^{-1} \mathbf{X}_f^T (\hat{\mathbf{o}}^{(f)}[t] \odot \mathbf{c}) \quad (14)$$

Substituting this into the expression for $\hat{\mathbf{x}}^{(f)}[t + 1]$, we can write

$$\hat{\mathbf{x}}^{(f)}[t + 1] = \text{sgn}\left(\mathbf{X}_f (\mathbf{X}_f^T \mathbf{X}_f)^{-1} \mathbf{X}_f^T (\hat{\mathbf{o}}^{(f)}[t] \odot \mathbf{c})\right) \quad (15)$$

Recall that our definition of $\hat{\mathbf{o}}^{(f)}[t]$ is given by (7).

3.1.1 Neural network interpretation

Suppose $\hat{\mathbf{x}}^{(f)}[t + 1]$ indicates the state of a population of neurons at time $t + 1$. Each neuron receives an input $\hat{\mathbf{o}}^{(f)}[t] \odot \mathbf{c}$, modified by synapses modeled as a row of the ‘‘weight matrix’’ $\mathbf{X}_f (\mathbf{X}_f^T \mathbf{X}_f)^{-1} \mathbf{X}_f^T$. This ‘‘synaptic current’’ is passed through the activation function $\text{sgn}(\cdot)$ in order to determine the output, which is either $+1$ or -1 . If the input to each neuron were instead $\hat{\mathbf{x}}^{(f)}[t]$, its own previous state, then what we would have is a Bipolar Hopfield Network (Hopfield, 1982) with a synaptic learning rule originally proposed by Personnaz, Guyon, and Dreyfus (Personnaz et al., 1986), the so-called ‘‘projection’’ rule. In our case however, rather than being autoassociative, in which $\hat{\mathbf{x}}^{(f)}[t + 1]$ is a direct function of $\hat{\mathbf{x}}^{(f)}[t]$, our dynamics are heteroassociative, basing the updates on the states of the *other* factors.

Moreover, we imagine F separate subpopulations of neurons which evolve together in time, each one responsible for estimating a different factor of \mathbf{c} . For now we are just specifying this as a discrete-time network in which updates are made one-at-a-time, but it can be extended as a continuous-valued, continuous-time dynamical system along the same lines as was done for Hopfield Networks (Hopfield, 1984). In that case, we can think about these F subpopulations of neurons evolving in a truly parallel way. Connecting the subpopulations together as we have specified has a dramatic effect on the way that $\hat{\mathbf{x}}^{(f)}[t]$ evolves compared to a classical Hopfield Network, which we discuss in the next section.

3.1.2 Algorithmic interpretation

The vector $\hat{\mathbf{o}}^{(f)}[t] \odot \mathbf{c}$ is a “suggestion” for $\hat{\mathbf{x}}^{(f)}[t]$ based on the current states of the *other* factors. The matrix $\mathbf{X}_f(\mathbf{X}_f^T\mathbf{X}_f)^{-1}\mathbf{X}_f^T$, when applied to any N -dimensional vector, produces the *Ordinary Least Squares* projection of that vector onto the linear subspace spanned by the columns of \mathbf{X}_f , which is precisely the space within which we must search for a factor. Therefore, $\hat{\mathbf{x}}^{(f)}[t+1]$ is a *bipolarized* Ordinary Least Squares projection of $\hat{\mathbf{o}}^{(f)}[t] \odot \mathbf{c}$ onto $\mathcal{R}(\mathbf{X}_f)$.

Another way of looking at the dynamics of a Resonator Circuit with OLS weights is that it is implementing a bipolarized version of the Alternating Least Squares algorithm we introduced in Section 2.3. Suppose we were to take the dynamics specified in (8) for making ALS updates to $\mathbf{a}_f[t+1]$, but we also bipolarize the vector $\hat{\mathbf{x}}^{(f)}[t+1]$. When the estimates $\hat{\mathbf{x}}^{(f)}[t+1]$ are bipolar, the vector $\hat{\mathbf{o}}^{(f)}[t]$ is bipolar and we can simplify the term $(\boldsymbol{\xi}^T\boldsymbol{\xi})^{-1}\boldsymbol{\xi}^T$:

$$\begin{aligned} \hat{\mathbf{o}}^{(f)}[t] \in \{-1, 1\}^N &\iff (\boldsymbol{\xi}^T\boldsymbol{\xi})^{-1}\boldsymbol{\xi}^T = (\mathbf{X}_f^T\text{diag}(\hat{\mathbf{o}}^{(f)}[t])^2\mathbf{X}_f)^{-1}\mathbf{X}_f^T\text{diag}(\hat{\mathbf{o}}^{(f)}[t]) \\ &= (\mathbf{X}_f^T\mathbf{X}_f)^{-1}\mathbf{X}_f^T\text{diag}(\hat{\mathbf{o}}^{(f)}[t]) \end{aligned} \quad (16)$$

The ALS update $\mathbf{a}_f[t+1] = (\boldsymbol{\xi}^T\boldsymbol{\xi})^{-1}\boldsymbol{\xi}^T\mathbf{c}$ is now *the same* as equation (14) – a Resonator Circuit with OLS weights is implementing a bipolarized version of Alternating Least Squares. It may be a bit of a misnomer to call this algorithm Bipolarized Alternating Least Squares because at each iteration it is *not* solving a least squares problem. To set $\mathbf{a}_f[t]$ according to (14) is to take the term $g(\mathbf{X}_f\mathbf{a}_f[t])$ present in $\frac{1}{2}\|\mathbf{c} - \hat{\mathbf{c}}\|_2^2$ and to treat the activation function *as if* it were linear. As a result, the iterates *do not always descend a loss function and the dynamics are not guaranteed to converge*. It is true that $\hat{\mathbf{c}} = \mathbf{c}$ is a fixed point of these dynamics, but this is not particularly comforting given that our starting point $\hat{\mathbf{x}}^{(f)}[0]$ will yield an estimate $\hat{\mathbf{c}}[0]$ that is likely to be very far from \mathbf{c} . Unlike Hopfield Networks, which have a Lyapunov function *certifying their global asymptotic stability*, no such function (that we know of) exists for a Resonator Circuit. We have observed trajectories that collapse to limit cycles and trajectories that do not seem to converge in any reasonable time. There is, however, a large and practical regime of operation where M is small enough that these non-converging trajectories are extremely rare. It is fairly simple to deal with these trajectories, making the model very useful in practice despite the lack of a convergence guarantee. It has also been argued in several places (see Van Vreeswijk and Sompolinsky (1996), for example) that cyclic or chaotic trajectories may be useful to a neural system, including in cases where there are multiple plausible states to entertain. This is just to say that we feel the lack of a

convergence guarantee is not a critical weakness of our model but rather an interesting and potentially useful characteristic. We attempted many different modifications to the model’s dynamics which would provably cause it to converge, but these changes always hindered its ability to solve the factorization problem. We emphasize that unlike all of the models in Section 2.3, a Resonator Circuit is *not* descending a loss function. Rather, it makes use of the fact that:

- Each iteration is a bipolarized ALS update – it *approximately* moves the state towards the Least Squares solution for each factor.
- The correct solution is a fixed point.
- There may be a sizeable ‘basin of attraction’ around this fixed point, which the iterates help us descend.
- The number of spurious fixed points (which do not give the correct factorization) is relatively small.

All of these properties we will attempt to establish in Section 4. We believe that this makes the model more capable of exploring the search space (without getting stuck in spurious fixed points) and that it does so by pursuing a relatively intuitive strategy of making ‘noisy’ Alternating Least Squares updates. For this reason, it may be appropriate in the future to compare a Resonator Circuit to algorithms from the literature on stochastic optimization.

3.2 Resonator Circuit with outer product weights

The matrix $\mathbf{X}_f(\mathbf{X}_f^T\mathbf{X}_f)^{-1}\mathbf{X}_f^T$ is $N \times N$, which can be enormous. Implementing a Resonator Circuit on a conventional computer may require that we not store this matrix directly, but rather only store each codebook matrix \mathbf{X}_f (which is of size $N \times M_f$) and instead compute $\mathbf{X}_f(\mathbf{X}_f^T\mathbf{X}_f)^{-1}\mathbf{X}_f^T$ on the fly. In this case, the computational expense of inverting the matrix $\mathbf{X}_f^T\mathbf{X}_f$ may be a concern (this matrix is called the Gram matrix of \mathbf{X}_f and it contains the inner products between each of the codevectors). As an aside, if M_f is quite large, it may be sensible to use a subroutine that computes $(\mathbf{X}_f^T\mathbf{X}_f)^{-1}\mathbf{X}_f^T$ based on the singular value decomposition of \mathbf{X}_f . This has the added benefit of being numerically more stable than computing $(\mathbf{X}_f^T\mathbf{X}_f)^{-1}$ directly. If the codevectors are orthonormal, the Gram matrix $\mathbf{X}_f^T\mathbf{X}_f$ is the identity \mathbf{I} . When N is large (roughly speaking $> 1,000$), and the codevectors are chosen randomly i.i.d. from $\{-1, 1\}^N$, then they will be *very nearly* orthogonal and $N\mathbf{I}$ is a very close approximation to $\mathbf{X}_f^T\mathbf{X}_f$. Therefore it may make sense to set the weight matrix according to $\mathbf{X}_f\mathbf{X}_f^T$, instead of $\mathbf{X}_f(\mathbf{X}_f^T\mathbf{X}_f)^{-1}\mathbf{X}_f^T$. Most readers will be familiar with the weight matrix $\mathbf{X}_f\mathbf{X}_f^T$ as the so-called “outer product” learning rule of classical Hopfield Networks (Hopfield, 1982). This has the nice interpretation of Hebbian learning (Hebb, 1949) in which the strength of synapses between any two neurons (represented by this weight matrix) depends solely on their pairwise statistics over some dataset, in this case the codevectors. This yields the dynamics of a Resonator Circuit with outer product weights:

$$\mathbf{a}_f[t + 1] = \mathbf{X}_f^T(\hat{\mathbf{o}}^{(f)}[t] \odot \mathbf{c}) \quad (17)$$

$$\hat{\mathbf{x}}^{(f)}[t + 1] = \text{sgn}\left(\mathbf{X}_f \mathbf{X}_f^T(\hat{\mathbf{o}}^{(f)}[t] \odot \mathbf{c})\right) \quad (18)$$

Whenever the codevectors deviate strongly from the approximate-orthogonality assumption, the behavior of the Ordinary Least Squares and outer product variants of Resonator Circuits may strongly differ. One immediate consequence is that the solution $\hat{\mathbf{c}} = \mathbf{c}$ is no longer guaranteed to be a fixed point – it is only likely to be one when each M_f is small enough. Other than that, it is hard to say which choice is appropriate for a particular set of codevectors. It may be the case that using weights given by the outer product will produce better trajectories for a particular problem. It is, however, almost always the case that using outer product weights will lead to much faster simulation and this is a clear choice when the codevectors are nearly orthogonal. We focus on this case in most of our results due to its relative analytical tractability and use in standard analysis of both Hopfield Networks and Vector Symbolic Algebras.

Another important note on practical implementation: the matrices \mathbf{X}_f consist of entries that are just $+1$ and -1 , so the only computations necessary to simulate this variant of Resonator Circuits are

- Binary comparison and binary accumulation (for computing $\mathbf{a}_f[t] = \mathbf{X}_f^T(\hat{\mathbf{o}}^{(f)}[t] \odot \mathbf{c})$)
- Integer - binary multiplication and integer sum (for computing the vector $\mathbf{X}_f \mathbf{a}_f[t]$)
- Integer sign (for computing $g(\cdot)$)

Computing hardware with very large binary and integer arithmetic circuits can simulate this model very quickly. As we will discuss in Section 4.6, the factorization can still be done even with significant corruption to the vector \mathbf{c} . For these reasons, this model (and more generally, distributed cognitive architectures) are a good fit for emerging device nanotechnologies, a topic discussed in more detail in Rahimi et al. (2017).

4 Results

We present a characterization of Resonator Circuits along three main directions. The first direction is the stability of the solutions $\mathbf{x}_\star^{(f)}$, which we relate to the stability of classical Hopfield networks. The second is a fundamental measure of factorization capability we call the “operational capacity”. The third is the speed with which factorizations are found. We argue that the marked difference in factorization performance between Resonator Circuits and the benchmark algorithms lies in the relative *scarcity of spurious fixed points* enjoyed by Resonator Circuit dynamics.

In each of the simulations in this section we choose codevectors randomly i.i.d. from the discrete uniform distribution over the vertices of the hypercube – each element of each codevector is a Rademacher random variable (assuming the value -1 with probability 0.5 and $+1$ with probability 0.5). We generate \mathbf{c} by choosing one vector at random from each of the F codebooks and then computing their Hadamard product. The reason we choose

vectors randomly is because it makes the analysis of performance somewhat easier and more standardized, and it is the setting in which most of the well-known results on Hopfield Network capacity apply – we will make a few connections to these results. It is also often the setting in which we use Vector Symbolic Architecture (Gayler, 2004) and therefore these results on random vectors are immediately applicable to a variety of existing works using this model.

4.1 Stable-solution capacity and percolated noise

Suppose $\hat{\mathbf{x}}^{(f)}[0] = \mathbf{x}_\star^{(f)}$ for all f (we initialize it to the correct factorization; this will also apply to any t at which the algorithm comes upon $\mathbf{x}_\star^{(f)}$ on its own). What is the probability that the state stays there – i.e. that the correct factorization is a fixed point of the dynamics? This is the basis of what researchers have called the “capacity” of Hopfield Networks, where $\mathbf{x}_\star^{(f)}$ are patterns that the network has been trained to store. We choose to call it the “stable-solution capacity” in order to distinguish it from operational capacity, which we define in Section 4.2. In general one may not care whether the state is completely stable – it may be tolerable that the dynamics flip some small fraction of the bits of $\mathbf{x}_\star^{(f)}$ as long as it does not move the state too far away from $\mathbf{x}_\star^{(f)}$. Amit, Gutfreund, and Sompolinsky (Amit et al., 1985, 1987) established that in Hopfield Networks, an avalanche phenomenon occurs where bitflips accumulate and the network becomes essentially useless for values of $M_f > 0.138N$, at which point the approximate bitflip probability is 0.0036. While we don’t attempt any of this complicated analysis on Resonator Circuits, we do derive an expression for the bitflip probability of any particular factor $\mathbf{x}_\star^{(f)}$ that accounts for bitflips which “percolate” from factor to factor through the vector $\hat{\mathbf{o}}^{(f)}[0] \odot \mathbf{c}$.

We first note that this analysis is necessary only for Resonator Circuits with outer product weights – Ordinary Least Squares weights guarantee that the solutions are stable. If $\hat{\mathbf{x}}^{(f)}[0] = \mathbf{x}_\star^{(f)}$ for all f , then factor 1 “sees” an input $\mathbf{x}_\star^{(1)}$ at time $t = 1$. The vector $\mathbf{X}_1(\mathbf{X}_1^T \mathbf{X}_1)^{-1} \mathbf{X}_1^T \mathbf{x}_\star^{(1)}$ is exactly $\mathbf{x}_\star^{(1)}$ by the definition of orthogonal projection. This is true as well for all subsequent factors, meaning that $\mathbf{x}_\star^{(f)}$ is a fixed point under these updates, which are the dynamics of a Resonator Circuit with Ordinary Least Squares weights. For a Resonator Circuit with outer product weights, we must examine the vector $\mathbf{\Gamma} := \mathbf{X}_f \mathbf{X}_f^T (\hat{\mathbf{o}}^{(f)}[0] \odot \mathbf{c})$ and the situation is significantly more complicated.

At issue is the probability that Γ_i has a sign different from $(\mathbf{x}_\star^{(f)})_i$, i.e. that there is a bitflip in any particular component of the updated state. We start by noting that for factor 1, this bitflip probability is the same as a Hopfield network. Readers familiar with the literature on Hopfield Networks will know that with N and M_f reasonably large (approximately $N \geq 1,000$ and $M_f \geq 50$) Γ_i can be well-approximated by a Gaussian with mean $(\mathbf{x}_\star^{(f)})_i (N + M_f - 1)$ and variance $(N - 1)(M_f - 1)$; see appendix G for a simple derivation. This is summarized as the *Hopfield bitflip probability* h_f :

$$\begin{aligned}
 h_f &:= Pr \left[(\hat{\mathbf{x}}^{(f)}[1])_i \neq (\mathbf{x}_\star^{(f)})_i \right] \\
 &= Pr \left[\text{sgn}(\Gamma_i) \neq (\mathbf{x}_\star^{(f)})_i \right] \\
 &= \Phi \left(\frac{-N - M_f + 1}{\sqrt{(N - 1)(M_f - 1)}} \right)
 \end{aligned} \tag{19}$$

Where Φ is the cumulative density function of the Normal distribution. Hopfield Networks are often specified with the diagonal of $\mathbf{X}_f \mathbf{X}_f^T$ set to all zeros (having “no self-connections”), in which case the bitflip probability is $\Phi\left(\frac{-N}{\sqrt{(N-1)(M_f-1)}}\right)$. For large N and M_f this is often simplified to $\Phi(-\sqrt{N/M_f})$, which may be the expression most familiar to readers. Keeping the diagonal of $\mathbf{X}_f \mathbf{X}_f^T$ makes the codevectors more stable (see appendix G) and while there are some arguments in favor of eliminating it, we have found Resonator Circuits to exhibit better performance by keeping these terms.

In Appendix G we derive the bitflip probability for an arbitrary factor in a Resonator Circuit with outer product weights. This probability depends on whether a component of the state has already been flipped by the previous $f - 1$ factors, which is what we call *percolated noise* passed between the factors, and which increases the bitflip probability. The four relevant probabilities are:

$$r_f := Pr\left[(\hat{\mathbf{x}}^{(f)}[1])_i \neq (\mathbf{x}_\star^{(f)})_i\right] \quad (20)$$

$$n_f := Pr\left[(\hat{\mathbf{o}}^{(f+1)}[0] \odot \mathbf{c})_i \neq (\mathbf{x}_\star^{(f+1)})_i\right] \quad (21)$$

$$r_{f'} := Pr\left[(\hat{\mathbf{x}}^{(f)}[1])_i \neq (\mathbf{x}_\star^{(f)})_i \mid (\hat{\mathbf{o}}^{(f)}[0] \odot \mathbf{c})_i = (\mathbf{x}_\star^{(f)})_i\right] \quad (22)$$

$$r_{f''} := Pr\left[(\hat{\mathbf{x}}^{(f)}[1])_i \neq (\mathbf{x}_\star^{(f)})_i \mid (\hat{\mathbf{o}}^{(f)}[0] \odot \mathbf{c})_i \neq (\mathbf{x}_\star^{(f)})_i\right] \quad (23)$$

Equation (20) is the probability of a bitflip compared to the correct value, the *Resonator bitflip probability*. Equation (21) gives the probability that the *next* factor will see a net bitflip, a bitflip which has percolated through the previous factors. Equations (22) and (23) give the probability of a bitflip conditioned on whether or not this factor sees a net bitflip, and they are *different*. It should be obvious that

$$r_f = r_{f'}(1 - n_{f-1}) + r_{f''}n_{f-1} \quad (24)$$

and also that

$$n_f = r_{f'}(1 - n_{f-1}) + (1 - r_{f''})n_{f-1} \quad (25)$$

We show via straightforward algebra in Appendix G that the conditional probabilities $r_{f'}$ and $r_{f''}$ can be written recursively in terms of n_f :

$$r_{f'} = \Phi\left(\frac{-N(1 - 2n_{f-1}) - (M_f - 1)}{\sqrt{(M_f - 1)(N - 1)}}\right) \quad (26)$$

$$r_{f''} = \Phi\left(\frac{-N(1 - 2n_{f-1}) + (M_f - 1)}{\sqrt{(M_f - 1)(N - 1)}}\right) \quad (27)$$

The fact that the bitflip probability has to be split between these two conditions and that there is a dependence on n_{f-1} is what makes this different from the bitflip probability for a Hopfield Network (compare equations (26) and (27) against equation (19)). But how much different? How much of an increased bitflip probability does any given factor suffer due to percolated noise from the other factors, compared to how much it would have had under its own dynamics as a Hopfield Network? Suppose there are F Hopfield Networks all evolving

under their own dynamics (they are not connected together). The probability h_f is the bitflip probability for the f th Hopfield Network, whereas the probability r_f is the bitflip probability for the f th factor of a Resonating Circuit. We are interested in the quantity $r_f - h_f$. Let us first note that for a Hopfield network *with self connections* the maximum bitflip probability is 0.02275, which occurs at $M_f = N$. The ratio M_f/N is what determines the bitflip probability. Please see Appendix G for an explanation. We plot h_f for 5 Hopfield Networks with $N = 100,000$ in Figure 1a. One can see that the curves all lie on top of one another – each factor has the same bitflip probability. Contrast this against Figure 1b where clearly the higher-numbered factors in a Resonator Circuit receive some percolated noise from lower-numbered factors and as a result have an increased bitflip probability. We show the *difference* between these two sets of curves in Figure 2.

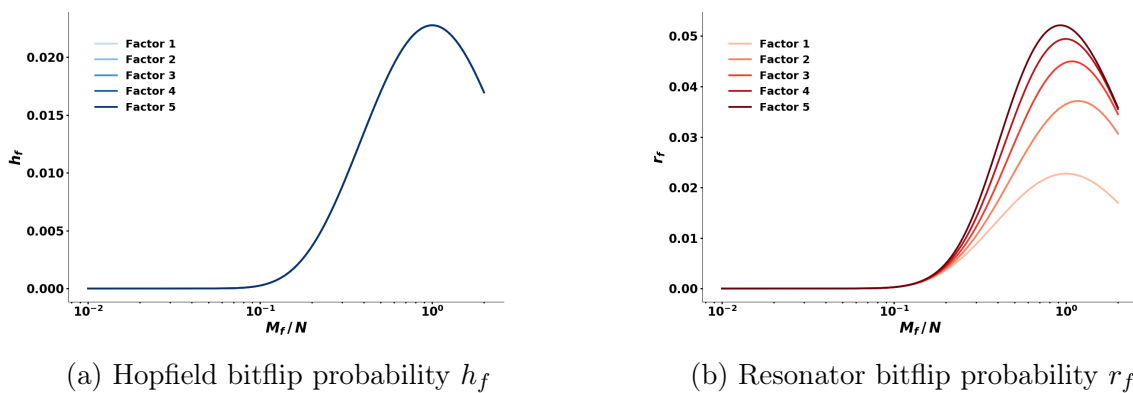


Figure 1: Comparing bitflip probabilities for $F = 5$ factors

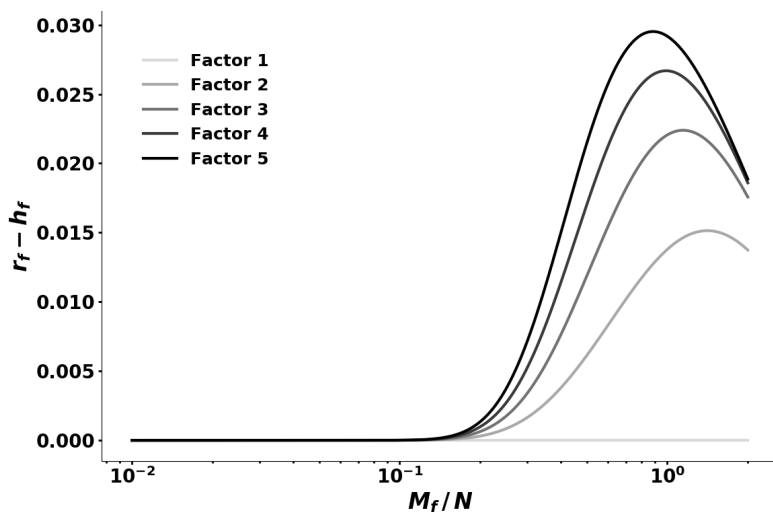


Figure 2: Extra bitflip probability $r_f - h_f$ due to percolated noise for $F = 5$ factors

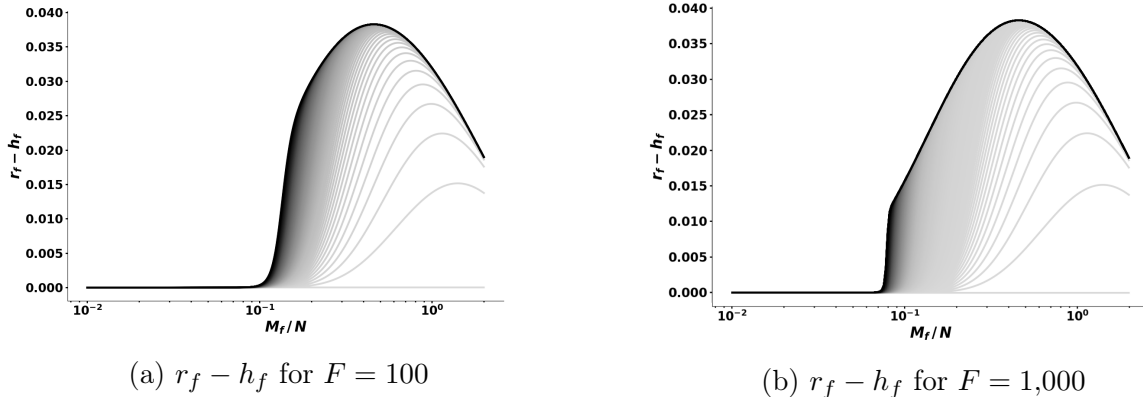


Figure 3: Limiting behavior of $r_f - h_f$ for 100 and 1,000 factors

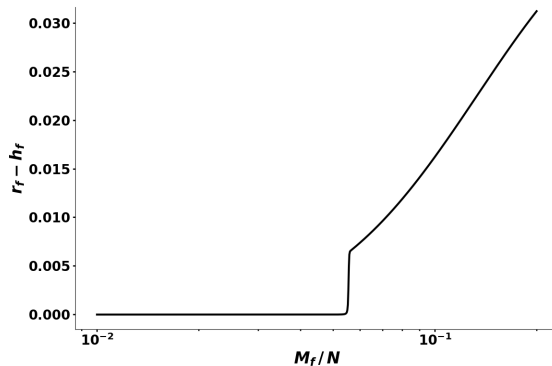


Figure 4: Extra bitflip probability $r_f - h_f$ for $F = 10,000$

To see if there is some limiting behavior, we simulated 100, 1,000, and 10,000 factors; the differences $r_f - h_f$ are shown in Figures 3 and 4. In Figure 4 there is clearly a phase change in residual bitflip probability which occurs at $M_f/N = 0.056$. In the Hopfield Network literature this is a very important number. It gives the point at which the codevectors transition away from being global minimizers of the Hopfield Network energy function. When M_f/N falls in between 0.056 and 0.138, the codevectors are only local minimizers, and there exist *spin-glass* states that have lower energy. What this result shows is that **for $M_f/N \leq 0.056$, the stability of a Resonator Circuit with outer product weights is the same as the stability of a Hopfield Network. For $M_f/N > 0.056$, percolated noise between the factors causes the Resonator circuit to be strictly less stable than a Hopfield Network.** We reiterate that this applies to outer product weights. When Resonator Circuit weights are set by Ordinary Least Squares, the solutions $\mathbf{x}_*^{(f)}$ are always stable.

4.2 Operational Capacity

We now define a new, more useful notion of capacity. This performance measure, called the *operational capacity*, gives an expression for the maximum size of factorization problem that can be solved with high probability. This maximum problem size, which we denote by M_{max} , varies as a function of the number of elements in each vector N and the number of factors F . It gives a very practical characterization of performance, and will form the basis of our comparison between Resonator Circuits and the benchmark algorithms we introduced in Section 2.3. When the problem size M is below the operational capacity of the algorithm, one can be quite sure that the correct factorization will be found efficiently.

Each algorithm we have introduced attempts to solve the factorization problem (1) by initializing the state of the estimates, $\hat{\mathbf{x}}^{(f)}[0]$, and letting the dynamics evolve until some termination criterion is met. It is possible that the final state of $\hat{\mathbf{x}}^{(f)}$ may not equal the correct factors $\mathbf{x}_\star^{(f)}$ at each and every component, but we can ‘decode’ each $\hat{\mathbf{x}}^{(f)}$ by looking for its nearest neighbor (with respect to Hamming distance or cosine similarity) among the vectors in its respective codebook \mathbb{X}_f . This distance computation involves only M_f vectors, rather than M , which was what we encountered in one of the brute-force strategies of Section 2. Compared to the other computations involved in finding the correct factorization out of M total possibilities, this last step of decoding has a very small cost. We define the total accuracy for any particular instantiation of the factorization problem to be the sum of accuracies for inferring each factor – if the nearest neighbor to $\hat{\mathbf{x}}^{(f)}$ is the correct factor, then this contributes $1/F$ to the total accuracy. For instance, correctly inferring one of three total factors gives a total accuracy of $1/3$, two of three is $2/3$, and three of three is 1.

Deriving the expected total accuracy appears to be quite challenging, especially for a Resonator Circuit, because it requires that we essentially predict how the nonlinear dynamics will evolve over time. There may be a region around each $\mathbf{x}_\star^{(f)}$ such that states in this region rapidly converge to $\mathbf{x}_\star^{(f)}$, the so-called basin of attraction, but our initial estimate $\hat{\mathbf{x}}_{(f)}[0]$ is likely not in the basin of attraction, and it is hard to predict when, if ever, the dynamics will enter this region. Even for Hopfield Networks, which obey much simpler dynamics than a Resonator Circuit, it is known that so-called “frozen noise” is built up in the network state, making the shapes of the basins highly anisotropic and difficult to analyze (Amari and Maginu, 1988). Essentially all of the analytical results on Hopfield Networks consider only the stability of the state $\mathbf{x}_\star^{(f)}$ as a (very poor) proxy for how the model behaves when it is initialized to other states. This less useful notion of capacity, the stable-solution capacity, was what we examined in the previous section.

We can, however, estimate the total accuracy by simulating many different factorization problems. This is just the fraction of factors that were correctly inferred over many, many trials. We remind the reader that our results in this paper pertain to factorization of randomly-drawn vectors which bear no particular correlational structure, but that notions of total accuracy and operational capacity would be relevant, and specific, to factorization of non-random vectors. We first note that for fixed vector dimensionality N , the empirical mean of the total accuracy depends strongly on M , the search space size. We can see this clearly in Figure 5. We show this phenomenon for a Resonator Circuit with outer product weights, but this general behavior is true for all of the algorithms under consideration – one can always make the search space large enough that expected total accuracy goes to zero.

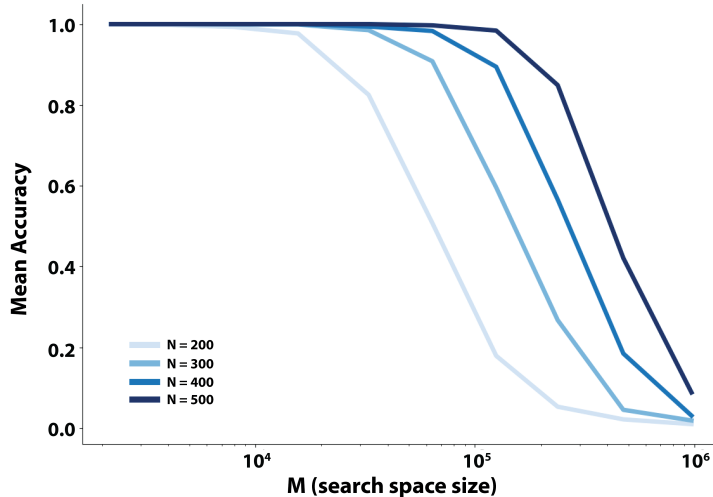


Figure 5: Total accuracy as a function of M for Resonator Circuit with outer product weights. Three factors ($F = 3$), average over 1,000 random trials.

Our notion of operational capacity is concerned with the M that causes expected total accuracy to drop below some value p . We see here that there are a range of values M for which the expected total accuracy is 1.0, beyond which this ceases to be the case. For all values of M within this range, the algorithm essentially always solves the factorization problem. We now define the most important metric in this paper, the *operational capacity* of algorithms for solving (1):

Definition 1. The $\{p, k\}$ operational capacity of a factorization algorithm that solves (1) is the largest search space size M_{max} such that the algorithm, when limited to a maximum number of iterations k , gives a total accuracy $\geq p$.

In this paper we estimate operational capacity when $p = 0.99$ ($\geq 99\%$ of factors were inferred correctly) and $k = 0.001M$ (the model can search over at most 1/1,000 of the entire search space). These choices are largely practical: $\geq 99\%$ accuracy makes the model very reliable in practice, and this operating point can be estimated from a reasonable number (3,000 to 5,000) of random trials. Setting $k = 0.001M$ allows the number of iterations to scale with the size of the problem, but restricts the algorithm to only consider a small fraction of the possible factorizations. While a Resonator Circuit has no guarantee of convergence, it almost always converges in far less than $0.001M$ iterations, so long as we stay in this high-accuracy regime.

Operational capacity is in general a function of N and F , as well as how ‘balanced’ the codebooks are (the degree to which they each contain the same number of codevectors). We will deal with this dependence explicitly when we estimate a scaling law for the operational capacity of Resonator Circuits, a main result of this paper. First, however, we compare the different algorithms under consideration on the basis of operational capacity.

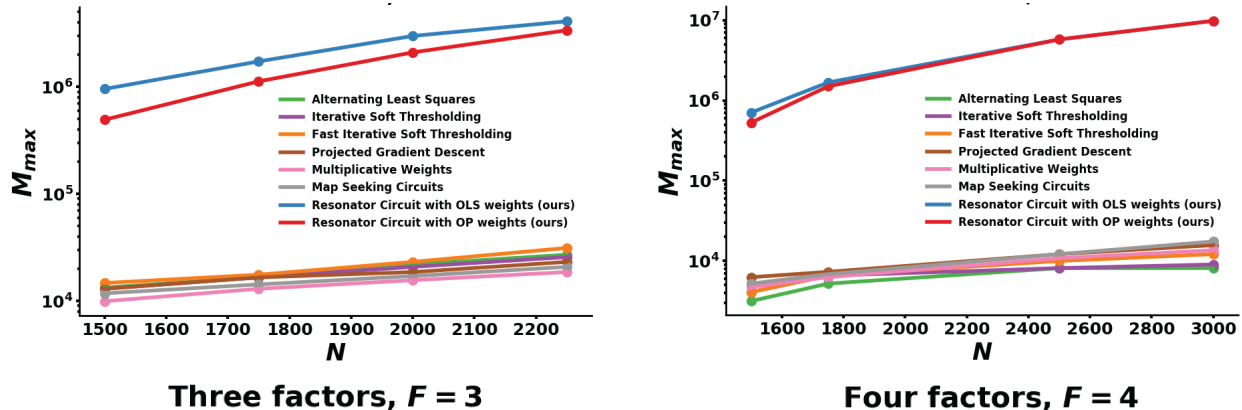


Figure 6: Operational capacity is dramatically higher for Resonator Circuits (blue and red above) than for any of the benchmark algorithms. These points represent the size of factorization problem that can be solved reliably.

4.2.1 Resonator Circuits have superior operational capacity

We estimated the operational capacity of Alternating Least Squares, Iterative Soft Thresholding, Fast Iterative Soft Thresholding, Projected Gradient Descent, Multiplicative Weights, and Map Seeking Circuits, in addition to the two variants of our algorithm. What is shown in Figure 6 is the operational capacity estimated on several thousand random trials, where we display M_{max} as a function of N for both three-factor problems and four-factor problems. One can see that **the operational capacity of Resonator Circuits is between two and three orders of magnitude greater than the operational capacity of the other algorithms**. Each of the benchmark algorithms has a slightly different operational capacity (due to the fact that they each have different dynamics and will, in general, find different solutions) but they are all similarly poor compared to the two variants of Resonator Circuit.

As N increases to 3,000 and beyond, the performance difference between the two variants of the Resonator Circuit starts to disappear, ostensibly due to the fact that $\mathbf{X}_f(\mathbf{X}_f^T\mathbf{X}_f)^{-1}\mathbf{X}_f^T \approx \mathbf{X}_f\mathbf{X}_f^T$. The two variants are different in general (and we have found that when the codevectors have significant similarities the Ordinary Least Squares variant performs better), but the simulations in this paper do not particularly highlight the difference between the two.

Except for Alternating Least Squares, each of the benchmark algorithms has at least one hyperparameter that must be chosen – we simulated many thousand random trials with a variety of hyperparameter settings for each algorithm and chose the hyperparameter values that performed best on average. We list these values for each of the algorithms in the Appendix. Each of the benchmark algorithms converge on their own and the tunable stepsizes make a comparison of the number of iterations non-standardized, so we did not impose a maximum number of iterations on these algorithms – the points shown represent the best the benchmark algorithms can do, even when not restricted to a maximum number of iterations. In fact, we experimented with many algorithms beyond those shown here in an attempt to find a competitive alternative to Resonator Circuits, but were unable to do so.

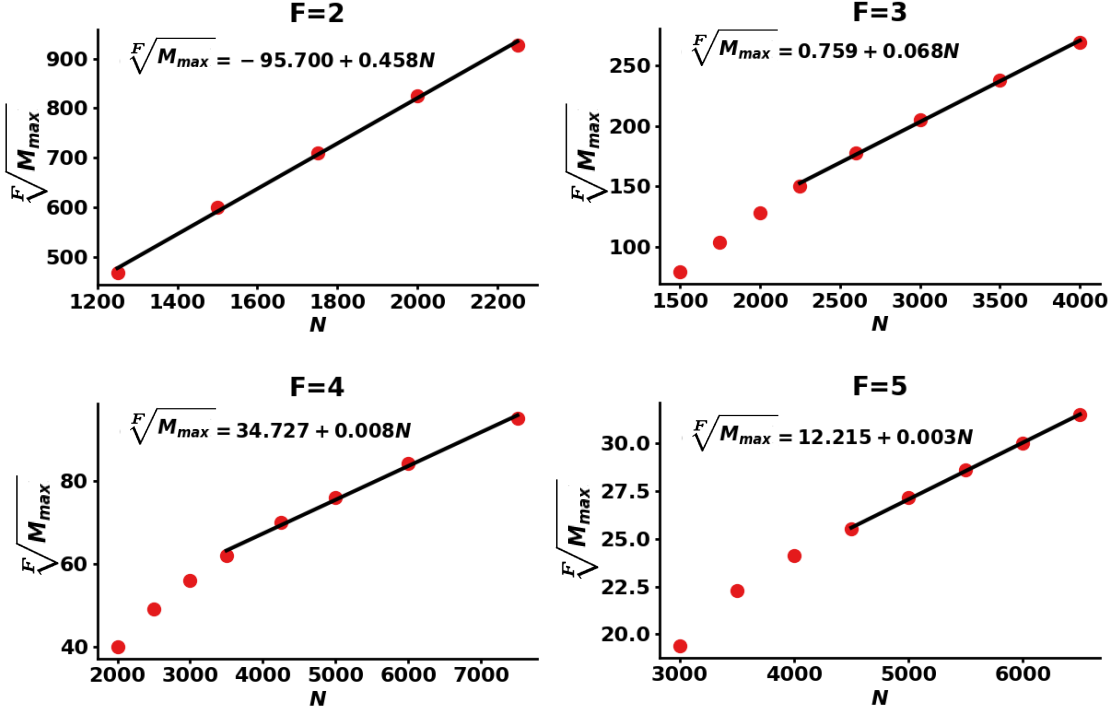


Figure 7: The f th root of M_{max} varies as a linear function N .

4.2.2 A scaling law for operational capacity of Resonator Circuits

The operational capacity is a very practical measure of performance, and we set out to estimate how it scales with parameters of the factorization problem. We are concerned with scaling in the limit of large N (where cross-talk noise between codevectors is well-approximated as Gaussian, see Section 4.1). The capacity scaling we find does not apply to small values of N .

We discovered a powerful and relatively simple scaling law for operational capacity which is illustrated by figure 7. The points are operational capacities estimated over many thousands of random trials and the lines give the best linear fits to a subset of these points – in the limit of large N we find that $\sqrt[F]{M_{max}}$ increases as a *linear* function of N . The slope of this relationship is heavily dependent on the number of factors F , which we find follows an inverse power-law in F (see figure 8). The linear dependence of $\sqrt[F]{M_{max}}$ on N implies that M_{max} scales according to N^F

$$\sqrt[F]{M_{max}} = \beta_0 + \beta_1 N \implies M_{max} = (\beta_0 + \beta_1 N)^F = \mathcal{O}(\beta_1^F N^F)$$

in the limit of large N . The values β_0 and β_1 are parameters of this linear scaling and depend in general on F , which one can see clearly in figure 7. From Figure 8 we estimate the expression for β_1 to be $\beta_1 = 25.74F^{-5.66}$. Substituting this into the expression for M_{max} , we have the main scaling law for operational capacity as a function of N and F :

$$M_{max} = \mathcal{O}(25.74F^{-5.66F} N^F) \quad (28)$$

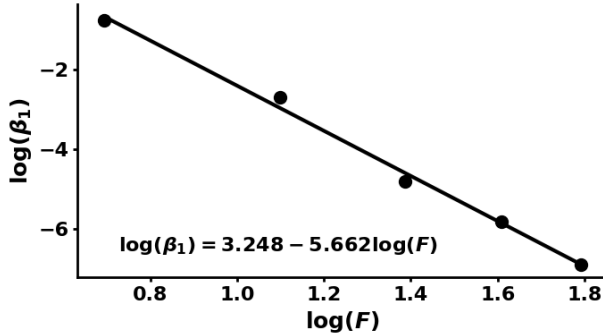


Figure 8: Parameter β_1 follows a power law in F : The exponent is the slope of this line and the multiplicative coefficient is $e^{3.248} \approx 25.74$

Capacity is highest when the codebooks \mathbb{X}_f each have the same number of codevectors ($M_1 = M_2 = \dots = M_F = \sqrt[F]{M}$), and this was the case for the operational capacity results we have shown so far. We chose this in order to have a simple standard for comparison among the different algorithms, but in general it is possible that the codebooks are unbalanced, so that we have the same $M = \prod_f M_f$ but $M_1 \neq M_2 \neq \dots \neq M_f$. In this case, capacity is lower than when the codebooks are balanced. We found that the most meaningful way to measure the degree of balance between codebooks was by the ratio of the smallest codebook to the largest codebook:

$$\gamma := \left(\min_f M_f \right) / \left(\max_f M_f \right) \quad (29)$$

For $\gamma \geq 0.2$ we found that the effect on $\sqrt[F]{M_{max}}$ was simply an additive factor which can be absorbed into a (slightly smaller) parameter β_0 . It does not appear to affect the value of β_1 and therefore the scaling for large N is still $\mathcal{O}(25.74F^{-5.66F}N^F)$. For extreme values of γ , where there is one codebook that is for instance 10 or 20 times larger than another, then both β_0 and β_1 are reduced, sometimes significantly. It is important to note, however, that the linear dependence of $\sqrt[F]{M_{max}}$ on N , and thus the power-law dependence of M_{max} on N , remains.

In summary, **equation (28) is a scaling law for the operational capacity M_{max} that holds for large N , values of $F \geq 2$, and for a moderate degree of imbalance between the codebooks. The operational capacity of Resonator Circuits is expansive and has a strong power-law dependence on the dimensionality of each vector N , allowing them to efficiently solve very large vector factorization problems.**

4.3 An explanation for differences in operational capacity

We believe that the sizable advantage in operational capacity enjoyed by Resonator Circuits can be partially attributed to the fact that their dynamics have relatively few spurious fixed points (those yielding incorrect factorizations) compared to each of the benchmark algorithms. Among the benchmark algorithms, we focus on Projected Gradient Descent (applied to the negative inner product with the simplex constraint) to illustrate this point. We will show that the correct factorization is always stable under Projected Gradient Descent

(as it is with the OLS variant of Resonator Circuits), but that incorrect factorizations are much more likely to be fixed points under Projected Gradient Descent.

4.3.1 Stability of the correct factorization

Coefficients \mathbf{a}_f are a fixed point of Projected Gradient Descent dynamics when the gradient at this point is exactly $\mathbf{0}$ or when it is in the nullspace of the projection operator. We write

$$\mathcal{N}(\mathcal{P}_{C_f}[\mathbf{x}]) := \{\mathbf{z} \mid \mathcal{P}_{C_f}[\mathbf{x} + \mathbf{z}] = \mathcal{P}_{C_f}[\mathbf{x}]\} \quad (30)$$

to denote this set of points. The nullspace of the projection operator is relatively small on the faces and edges of the simplex, but it becomes somewhat large at the vertices. The nullspace of the projection operator at a vertex of the simplex ($\mathbf{a}_f = \mathbf{e}_i$) is an intersection of halfspaces (each halfspace given by an edge of the simplex). We can compactly write the nullspace at a vertex with the following expression:

$$\mathcal{N}(\mathcal{P}_{\Delta_{M_f}}[\mathbf{e}_i]) = \{\mathbf{z} \mid \bigcap_{j \neq i} (\mathbf{e}_i - \mathbf{e}_j)^T \mathbf{z} \geq 1\} \quad (31)$$

An equivalent way to express the nullspace is

$$\mathcal{N}(\mathcal{P}_{\Delta_{M_f}}[\mathbf{e}_i]) = \{\mathbf{z} \mid z_j \leq z_i - 1 \quad \forall j \neq i\} \quad (32)$$

In other words, for a vector to be in the nullspace at \mathbf{e}_i , the i th element of the vector must be the largest by a margin of 1 or more. This condition is met for the vector $-\nabla_{\mathbf{a}_f} \mathcal{L}$ at the correct factorization, since $-\nabla_{\mathbf{a}_f} \mathcal{L} = \mathbf{X}_f^T (\hat{\mathbf{o}}^{(f)}[0] \odot \mathbf{c}) = \mathbf{X}_f^T \mathbf{x}_*^{(f)}$. This vector has a value N for the component corresponding to $\mathbf{x}_*^{(f)}$ and values that are $\leq N - 1$ for all the other components. Thus, the correct factorization (the solution to (1) and global minimizer of (5)) is always a fixed point under the dynamics of Projected Gradient Descent (PGD).

4.3.2 Stability of incorrect factorizations

Suppose we initialize the algorithm to a factorization which does not solve (1) – we have chosen a set of vectors from the codebooks, but they don't produce \mathbf{c} . Based on the assumption that each codevector was chosen randomly, the vector $\hat{\mathbf{o}}^{(f)}[0] \odot \mathbf{c}$ will be a *completely random bipolar vector*. So long as M_f is not too close to N , $\hat{\mathbf{o}}^{(f)}[0] \odot \mathbf{c}$ will be nearly orthogonal to every vector in \mathbb{X}_f and its projection onto $\mathcal{R}(\mathbf{X}_f)$ will be small, with each component equally likely to be positive or negative. Therefore, under the dynamics of a Resonator Circuit with OLS weights, each component will flip its sign compared to $\hat{\mathbf{o}}^{(f)}[0] \odot \mathbf{c}$ with probability $\frac{1}{2}$ and therefore $\hat{\mathbf{o}}^{(f)}[0] \odot \mathbf{c}$ will remain unchanged with probability $\frac{1}{2^N}$. This is obviously quite small for N of any reasonable size – suboptimal factorizations are *very* unlikely to be a fixed points. The same is true for a Resonator Circuit with OP weights because $\mathbf{\Gamma} = \mathbf{X}_f \mathbf{X}_f^T (\hat{\mathbf{o}}^{(f)}[0] \odot \mathbf{c})$ has elements that are approximately Gaussian with mean zero – again each component is equally likely to flip or not flip compared to $\hat{\mathbf{o}}^{(f)}[0] \odot \mathbf{c}$.

Contrast this against Projected Gradient Descent. We recall from (32) that the requirement for \mathbf{e}_i to be a fixed point is that the i th component of the gradient at this point be

largest by a margin of 1 or more. *This is a much looser condition than we had for Resonator Circuits* – such a scenario will actually occur with probability $1/M_f$ for any of these arbitrary spurious factorizations. We can see from this argument that with Resonator Circuits, suboptimal factorizations will be fixed points with probability $\frac{1}{2^N}$ while with Projected Gradient Descent this will occur with probability $\frac{1}{M_f}$. This does not directly address the case when $\hat{\mathbf{o}}^{(f)}[0] \odot \mathbf{c}$ is *partially* correlated with one of the codevectors, but it is fair to say that for a Resonator Circuit, such a state will be a fixed point with a probability in the interval $[\frac{1}{2^N}, 1]$ while for Projected Gradient Descent the interval is $[\frac{1}{M_f}, 1]$. Therefore, Projected Gradient Descent is much more likely to exhibit spurious fixed points. While the details differ slightly, our experience indicates that this property is shared by each one of the benchmark algorithms.

4.3.3 Basins of attraction for benchmark algorithms

It may be that while there are sizable basins of attraction around the correct factorization, moving through the interior of the hypercube causes state trajectories to fall into the basin corresponding to a spurious fixed point. In a normal setting for several of the optimization-based approaches, we initialize \mathbf{a}_f to be at the center of the simplex, indicating that each of the factorizations is equally likely. Suppose we were to initialize \mathbf{a}_f so that it is just slightly nudged toward one of the simplex vertices. We might nudge it toward the correct vertex (the one given by \mathbf{a}_f^*) or we might nudge it toward any of the other vertices, away from \mathbf{a}_f^* . We can parameterize this with a single scalar θ and \mathbf{e}_i chosen uniformly among the possible vertices:

$$\mathbf{a}_f[0] = \theta \mathbf{e}_i + (1 - \theta) \frac{1}{M_f} \mathbf{1} \quad | \quad \theta \in [0, 1], \quad i \sim \mathcal{U}\{1, M_f\}$$

We ran a simulation with $N = 1500$ and $M_1 = M_2 = M_3 = 50$, at which Projected Gradient Descent and Multiplicative Weights both have a total accuracy around 0.5. We created 5,000 random factorization problems, initializing the state slightly towards the correct factorization and then initializing it slightly towards a randomly chosen spurious factorization. The dynamics were allowed to run until convergence and then the implied factorization was decoded using the nearest-neighbor among the codevectors, as we introduced in Section 4.2.

What Figure 9 shows is that by moving just a small distance toward the correct vertex, we very quickly fall into its basin of attraction. However, moving toward any of the other vertices is actually somewhat likely to take us into a spurious basin of attraction (where the converged state is decoded into an incorrect factorization). The space is *full* of these bad directions. It would be very lucky indeed to start from the center of the simplex and move immediately toward the solution – it is far more likely that initial updates take us somewhere else in the space, toward one of the other vertices, and this plot shows that these trajectories often get pulled towards a spurious fixed point. What we are demonstrating here is that empirically, the interior of the hypercube is somewhat treacherous from an optimization perspective, and this might lie at the heart of why the benchmark algorithms fail.

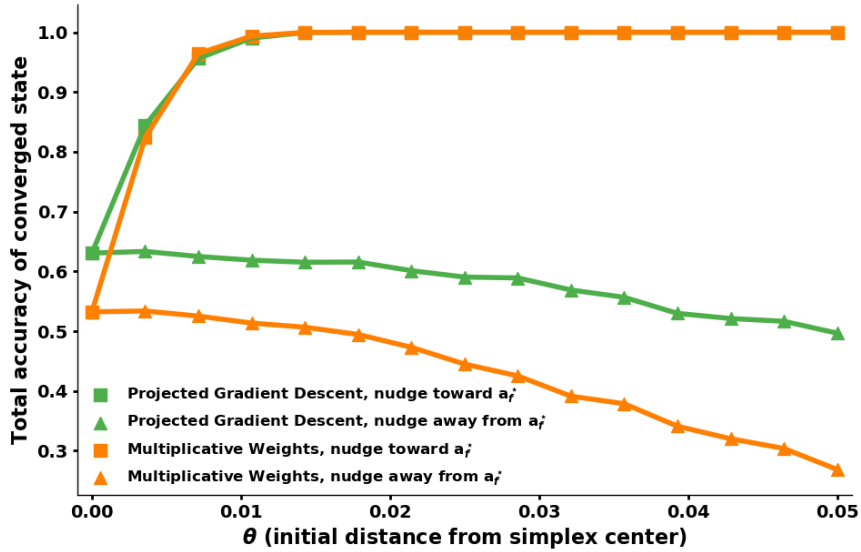


Figure 9: States in hypercube interior get pulled into spurious basins of attraction

4.4 Search efficiency

If a Resonator Circuit is not consistently descending an energy function, is it just aimlessly wandering around the space, trying every possible factorization until it finds the correct one? Figure 10 shows that it is not. We plot the mean number of iterations over 5,000 random trials, as a fraction of M , the search space size. This particular plot is based on a Resonator Circuit with outer product weights and $F = 3$. In the high-performance regime where M is below operation capacity, the number of iterations is far less than the $0.001M$ cutoff we used in the simulations of Section 4.2 – the algorithm is only ever considering a tiny fraction of the possible factorizations before it finds the solution.

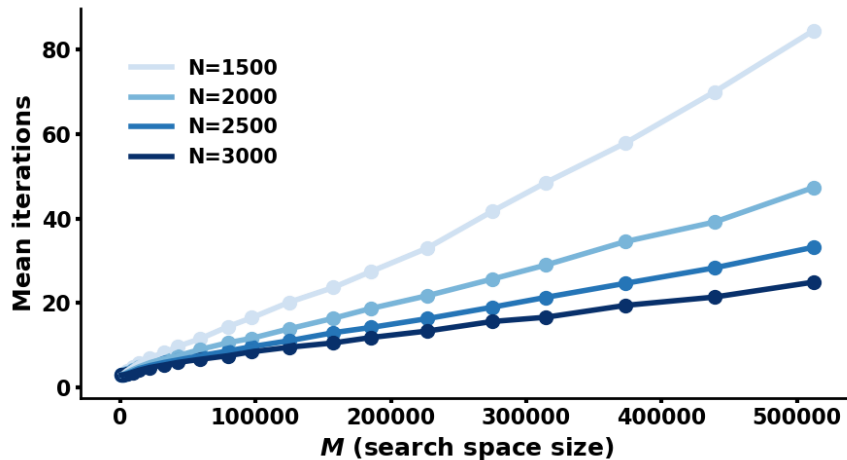
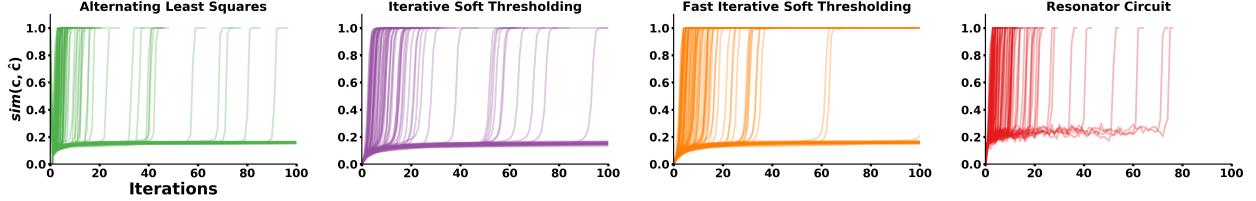
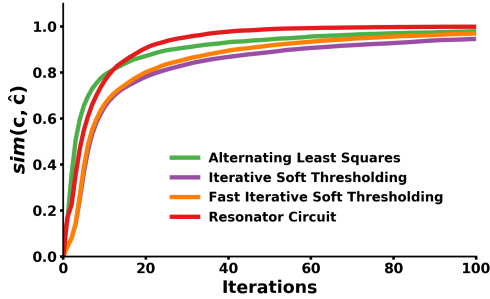


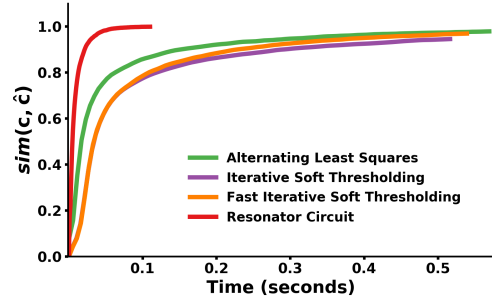
Figure 10: Iterations until convergence, Resonator Circuit with outer product weights and $F = 3$.



(a) Convergence traces for 100 randomly-drawn factorization problems – each line is the cosine similarity between \mathbf{c} and $\hat{\mathbf{c}}$ over iterations of the algorithm. Each of the four algorithms is run on *the same* 100 factorization problems. All of the instances are solved by the Resonator Circuit, whereas a sizeable fraction (around 30%) of the instances are not solved by the benchmark algorithms, at least within 100 iterations.



(b) Avg. cosine similarity vs. iteration number (only trials with accuracy 1.0)



(c) Avg. cosine similarity vs. wall-clock time (only trials with accuracy 1.0)

Figure 11: Our benchmark of factorization speed. Implementation in Python with NumPy. Run on machine with Intel Core i7-6850k processor and 32GB RAM. We generated 5,000 random instantiations of the factorization problem with $N = 1500$, $F = 3$, and $M_f = 40$, running each of the four algorithms in turn. Figure 11a gives a snapshot of 100 randomly selected trials. Figures 11b and 11c show average performance *conditioned on the algorithms finding the correct factorization*.

Section 4.2.1 compared the operational capacity of different algorithms and showed that compared to the benchmarks, Resonator Circuits can solve much larger factorization problems. This is in the sense that the dynamics eventually converge (with high probability) on the correct factorization while, the dynamics of the other algorithms converge on spurious factorizations. This result, however, does not directly demonstrate the relative speed with which factorization are found in terms of either the number of iterations or the amount of time to convergence. We set up a benchmark to determine the relative speed of Resonator Circuits and our main finding is depicted in Figure 11. What these plots indicate is that **measured in number of iterations, Resonator Circuits are comparable to the benchmark algorithms. However, due to the nearly 5x lower per-iteration cost of Resonator Circuits with outer product weights, this variant is significantly faster in terms of wall-clock time.** Resonator Circuits with outer product weights utilize very simple arithmetic operations and this explains the difference between Figures 11b and 11c.

4.5 Dynamics that do not converge

One must be prepared for the possibility that the dynamics of a Resonator Circuit will not converge. Fortunately, for M below the $p = 0.99$ operational capacity, these will be exceedingly rare. We simulated the random vector factorization problem and identified three major regimes of different convergence behavior:

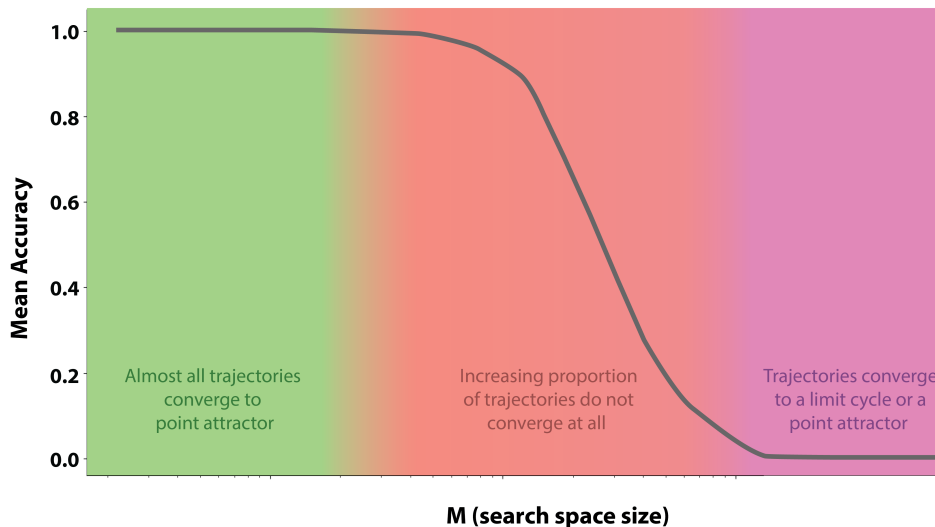


Figure 12: Regimes of non-convergence

- For M small enough, almost all trajectories converge, and moreover they converge to the correct factorization. Any incorrect factorizations are due to trajectories which fell into a limit cycle or did not converge at all in the allotted time – if the circuit converged on its own, one can be confident this was because it found the correct factorization.
- As M increases, non-converging trajectories appear in greater proportion and yield incorrect factorizations. Any trajectories which converge on their own continue to yield the correct factorization, but these become less common.
- Beyond some saturation value M_{sat} , limit cycles appear, almost all of which correspond to incorrect factorizations. As M_f approaches N , the synaptic matrix is a basis for all of \mathbb{R}^N and *all states are stable* (but give incorrect factorizations).

Limit cycles of any length may appear, although they tend to be skewed towards small cycle lengths. One can check for the existence of a limit cycle of size L with a cyclic buffer that stores L past states – this has relatively low overhead compared to the other Resonator Circuit computations and it may be worth it in practice to keep some small number of these buffers in order to catch small limit cycles. Our intuition about what happens in the middle section of Figure 12 is that the basins of attraction become very narrow and hard to find for the Resonator Circuit dynamics. The algorithm will wander, since it has so few spurious fixed points, but not be able to find any basin of attraction.

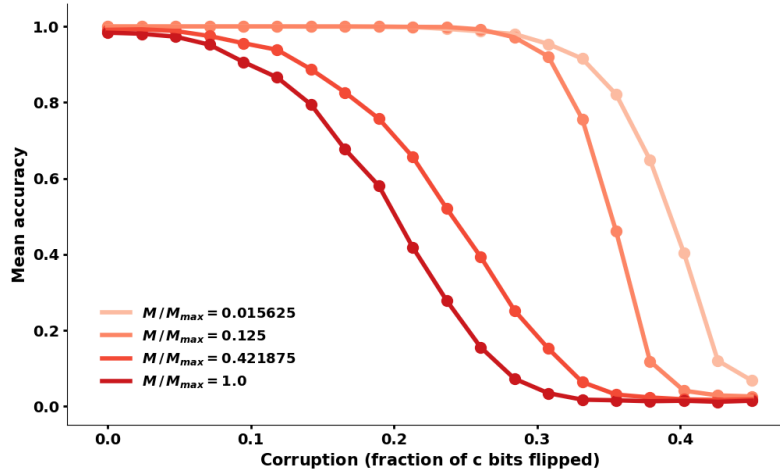


Figure 13: Factoring a corrupted \mathbf{c}

4.6 Factoring a ‘noisy’ composite vector

Our assumption has been that one combination of codevectors from our codebooks \mathbb{X}_f generates \mathbf{c} exactly. What if this is not the case? Perhaps the vector we are given for factorization has had some proportion ζ of its components flipped, that is, we are given $\tilde{\mathbf{c}}$ where $\tilde{\mathbf{c}}$ differs from \mathbf{c} in exactly $\lfloor \zeta N \rfloor$ places. The vector \mathbf{c} has a factorization based on our codebooks but $\tilde{\mathbf{c}}$ does not. We should hope that a Resonator Circuit will return the factors of \mathbf{c} so long as the corruption is not too severe. This is an especially important capability in the context of Vector Symbolic Architectures, where $\tilde{\mathbf{c}}$ will often be the result of some algebraic manipulations that generate noise and corrupt the original \mathbf{c} to some degree. We show in Figure 13 that a Resonator Circuit can still produce the correct factorization even after a sizable number of bits have been flipped. This robustness is more pronounced when the number of factorizations is well below operational capacity, at which point the model can often still recover the correct factorization even when 30% of the bits have been flipped.

4.7 Superposition of composite vectors

Suppose that, contrary to the way we have defined our problem (1), we instead generate two or more composite vectors from the factors available, called $\mathbf{c}_1, \mathbf{c}_2, \dots, \mathbf{c}_K$, and add them together to generate the vector \mathbf{c}

$$\mathbf{c} = \mathbf{c}_1 + \mathbf{c}_2 + \dots + \mathbf{c}_K$$

The task is still to decompose \mathbf{c} , but it now contains multiple composites in superposition. If one applies a Resonator Circuit to this (now integer-valued) \mathbf{c} , a very natural thing happens. The model picks one of the \mathbf{c}_k and factors it. There are ‘noise’ terms in \mathbf{c} due to the other composite vectors, so the task is not as easy as before, but it is remarkable how well this still works. In high enough dimensions, the noise due to the presence of these other composites

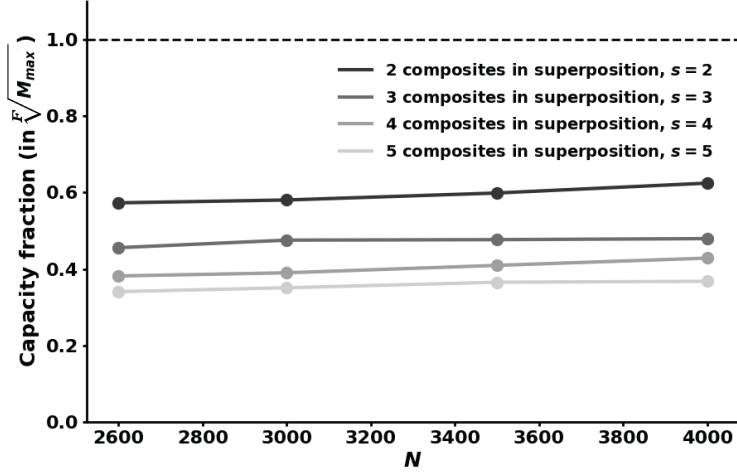


Figure 14: Composites in superposition reduce capacity by a constant multiplicative factor

is approximately Gaussian and has a small variance, so that a Resonator Circuit can still find directions in the space that lead to fixed points and the correct factorization.

Once the model has converged, its estimate $\hat{\mathbf{x}}^{(1)} \odot \hat{\mathbf{x}}^{(2)} \odot \dots \odot \hat{\mathbf{x}}^{(F)}$ can be subtracted from \mathbf{c} and the circuit can be run again. We call this procedure “explaining away”. The topic deserves more detailed treatment in a later work, but for now we just establish empirically the effect of this superposition noise on the operational capacity of the Resonator Circuits – we amend the capacity scaling law estimated in Section 4.2.2 to include dependence on the number of composites in superposition.

In each random instantiation of the problem, the order in which composite vectors are chosen during the steps of explaining away will change, so without loss of generality we just look at the total accuracy of decoding \mathbf{c}_1 – in whichever step of explaining away our estimate $\hat{\mathbf{x}}^{(1)} \odot \hat{\mathbf{x}}^{(2)} \odot \dots \odot \hat{\mathbf{x}}^{(F)}$ is closest to \mathbf{c}_1 , we take that step as the one assigned to \mathbf{c}_1 and calculate the decoding accuracy in this step.

What Figure 14 shows is that $\sqrt[F]{M_{max}}$ is proportional to a parameter $\alpha \leq 1.0$, which depends strongly on the number of composites in superposition. That is, we have

$$\sqrt[F]{M_{max}} = \alpha(\beta_0 + \beta_1 N) \implies M_{max} = \alpha^F (\beta_0 + \beta_1 N)^F = \mathcal{O}(\alpha^F \beta_1^F N^F)$$

The parameter α has, in fact, an inverse power-law dependence on K (the number of composites in superposition) in much the same way that β_1 did in terms of F . This fact is evident from figure 15. The expression for α is then $\alpha = 0.875K^{-0.558}$. Substituting this into our amended scaling law and combining terms, we have a new scaling law that accounts for composites in superposition:

$$M_{max} = \mathcal{O}\left(25.74 \left(\frac{0.874F^{-5.66}N}{K^{0.558}}\right)^F\right) \quad (33)$$

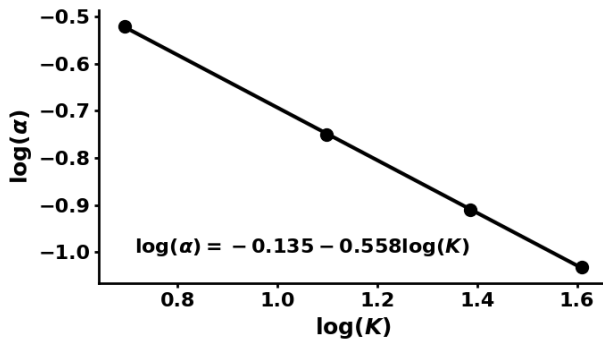


Figure 15: Parameter α follows a power law in K : The exponent is the slope of this line and the multiplicative coefficient is $e^{-0.135} \approx 0.874$

5 Discussion

There are several prior works involving some aspect of factorization that we would like to mention here, but we emphasize that each one of them deals with a problem or approach that is distinct from what we have introduced in this paper. Bidirectional Associative Memory, proposed by Kosko (1988), is an extension of Hopfield Networks that stores *pairs* of factors in a matrix using the outer product learning rule. The composite object is a matrix, rather than a vector, and is much closer to a particular type of tensor decomposition called the ‘CP decomposition’, which we elaborate on in Appendix A. Besides the fact that this model applies only to *two* factor problems, its dynamics are different from ours and its capacity is relatively low (Kobayashi et al., 2002). Subsequent efforts to extend this model to factorizations with 3 or more factors (Huang and Hagiwara, 1999; Kobayashi et al., 2002) have had very limited success and still rely on matrices that connect pairs of factors rather than a single multilinear product, which we have in our model. Bilinear Models of Style and Content (Tenenbaum and Freeman, 2000) was an inspiration for us in deciding to work on factorization problems. This paper applies a different type of tensor decomposition, a ‘Tucker decomposition’ (again see Appendix A), to a variety of different real-valued datasets using what appears to be in one case a closed-form solution based on the Singular Value Decomposition, and in the other case a variant of Alternating Least Squares. In that sense, their method is different from ours, the factorization problem is itself different, and they consider only pairs of factors. Memisevic and Hinton (2010) revisits the Tucker decomposition problem, but factors the ‘core’ tensor representing interactions between factors in order to make estimation more tractable. They propose a Boltzmann Machine that computes the factorization and show some results on modeling image transformations. Finally, there is a large body of work on matrix factorization of the form $\mathbf{V} \approx \mathbf{WH}$, the most well-known of which is probably Non-negative Matrix Factorization (Lee and Seung, 2001). The matrix \mathbf{V} can be thought of a sum of outer products, so this is really a type of CP decomposition with an additional constraint on the sign of the factors. Different still is the fact that \mathbf{W} is often interpreted as a basis for the columns of \mathbf{V} , with \mathbf{H} containing the coefficients of each column with respect to this basis. In this sense, vectors are being *added* to explain \mathbf{V} , rather than combined multiplicatively – Non-negative Matrix Factorization is much closer to Sparse Coding.

This work can be built upon in several directions. First, we intend to explore the Complex Resonating Circuit, a model in which vectors are complex-valued, with each component a unit-magnitude phasor. A recent theory of *sparse* phasor associative memories (Frady and Sommer, 2019) may be relevant to this direction, and allow us to perform factorization with a network of spiking neurons. Second, we have treated the codebook matrix as a one-hot representation of the factors, but a natural extension is to treat it as a basis for each factor – we have some preliminary results indicating that this is indeed a powerful approach. Third, we would like to consider Tucker decomposition problems and revisit Tenenbaum and Freeman (2000) and Memisevic and Hinton (2010) through the lens of Resonating Circuits. Fourth, we would like to scale up an image factorization example that factorizes complex 3D scenes via a mapping from image space to a latent space in which the factorization takes place.

6 Acknowledgements

We would like to thank members of the Redwood Center for Theoretical Neuroscience for helpful discussions, in particular Pentti Kanerva, whose work on Vector Symbolic Algebras originally motivated this project. We also thank Carson Kent for helpful comments, including pointing us to the Multiplicative Weights algorithm. This work was generously supported by a National Science Foundation Graduate Research Fellowship under grant number DGE1106400 and in part by the Semiconductor Research Corporation, under E2CDA-NRI, a program sponsored by NERC and NIST.

References

- Adelson, E. H. and Pentland, A. P. (1996). The perception of shading and reflectance. *Perception as Bayesian inference*, pages 409–423.
- Amari, S.-I. and Maginu, K. (1988). Statistical neurodynamics of associative memory. *Neural Networks*, 1(1):63–73.
- Amit, D. J., Gutfreund, H., and Sompolinsky, H. (1985). Storing infinite numbers of patterns in a spin-glass model of neural networks. *Physical Review Letters*, 55(14):1530.
- Amit, D. J., Gutfreund, H., and Sompolinsky, H. (1987). Information storage in neural networks with low levels of activity. *Physical Review A*, 35(5):2293.
- Arathorn, D. W. (2001). Recognition under transformation using superposition ordering property. *Electronics Letters*, 37(3):164–166.
- Arathorn, D. W. (2002). *Map-seeking circuits in visual cognition: A computational mechanism for biological and machine vision*. Stanford University Press, Stanford, CA.
- Arora, S., Hazan, E., and Kale, S. (2012). The multiplicative weights update method: a meta-algorithm and applications. *Theory of Computing*, 8(1):121–164.
- Barrow, H. and Tenenbaum, J. (1978). Recovering intrinsic scene characteristics from images. *Computer Vision Systems*, 2:3–26.
- Beck, A. and Teboulle, M. (2009). A fast iterative shrinkage-thresholding algorithm for linear inverse problems. *SIAM journal on imaging sciences*, 2(1):183–202.
- Boucheron, S., Lugosi, G., and Massart, P. (2013). *Concentration inequalities*. Oxford University Press, Oxford. A nonasymptotic theory of independence, with a foreword by Michel Ledoux.
- Bredies, K. and Lorenz, D. A. (2008). Linear convergence of iterative soft-thresholding. *Journal of Fourier Analysis and Applications*, 14(5-6):813–837.
- Cadieu, C. F. and Olshausen, B. A. (2012). Learning intermediate-level representations of form and motion from natural movies. *Neural computation*, 24(4):827–866.
- Carroll, J. D. and Chang, J.-J. (1970). Analysis of individual differences in multidimensional scaling via an n-way generalization of “eckart-young” decomposition. *Psychometrika*, 35(3):283–319.
- Carroll, J. D., Pruzansky, S., and Kruskal, J. B. (1980). Candelinc: A general approach to multidimensional analysis of many-way arrays with linear constraints on parameters. *Psychometrika*, 45(1):3–24.
- Condat, L. (2016). Fast projection onto the simplex and the l1 ball. *Mathematical Programming*, 158(1-2):575–585.

- Daubechies, I., Defrise, M., and De Mol, C. (2004). An iterative thresholding algorithm for linear inverse problems with a sparsity constraint. *Communications on Pure and Applied Mathematics: A Journal Issued by the Courant Institute of Mathematical Sciences*, 57(11):1413–1457.
- De Lathauwer, L., De Moor, B., and Vandewalle, J. (2000). A multilinear singular value decomposition. *SIAM journal on Matrix Analysis and Applications*, 21(4):1253–1278.
- Duchi, J., Shalev-Shwartz, S., Singer, Y., and Chandra, T. (2008). Efficient projections onto the l_1 -ball for learning in high dimensions. In *Proceedings of the 25th international conference on Machine learning*, pages 272–279. ACM.
- Eliasmith, C., Stewart, T. C., Choo, X., Bekolay, T., DeWolf, T., Tang, Y., and Rasmussen, D. (2012). A large-scale model of the functioning brain. *Science*, 338(6111):1202–1205.
- Emruli, B., Gayler, R. W., and Sandin, F. (2013). Analogical mapping and inference with binary spatter codes and sparse distributed memory. In *The 2013 international joint conference on neural networks (IJCNN)*, pages 1–8. IEEE.
- Fraday, E. P., Kent, S., Kanerva, P., Olshausen, B., and Sommer, F. (2018a). Cognitive neural systems for disentangling compositions. In *Cognitive Computing 2018 (extended abstract)*.
- Fraday, E. P., Kent, S. J., and Olshausen, B. A. (2018b). A recurrent neural network model for factoring distributed representations. In *Computational and systems neuroscience (CoSyNe '18) (extended abstract) [link]*.
- Fraday, E. P. and Sommer, F. T. (2019). Robust computation with rhythmic spike patterns. *arXiv preprint arXiv:1901.07718*, 1901.07718.
- Gayler, R. W. (1998). Multiplicative binding, representation operators & analogy (workshop poster). In Holyoak, K., Gentner, D., and Kokinov, B., editors, *Advances in analogy research: Integration of theory and data from the cognitive, computational, and neural sciences*.
- Gayler, R. W. (2004). Vector symbolic architectures answer jackendoff’s challenges for cognitive neuroscience. *arXiv preprint arXiv:cs/0412059*.
- Gedeon, T. and Arathorn, D. (2007). Convergence of map seeking circuits. *Journal of Mathematical Imaging and Vision*, 29(2-3):235–248.
- Harker, S., Vogel, C. R., and Gedeon, T. (2007). Analysis of constrained optimization variants of the map-seeking circuit algorithm. *Journal of Mathematical Imaging and Vision*, 29(1):49–62.
- Harshman, R. A. (1970). Foundations of the parafac procedure: Models and conditions for an ‘explanatory’ multimodal factor analysis. Technical Report UCLA Working Papers in Phonetics, 16, 1-84, University of California, Los Angeles.

- Hazan, E. et al. (2016). Introduction to online convex optimization. *Foundations and Trends in Optimization*, 2(3-4):157–325.
- Hebb, D. (1949). The organization of behavior; a neuropsychological theory.
- Held, M., Wolfe, P., and Crowder, H. P. (1974). Validation of subgradient optimization. *Mathematical programming*, 6(1):62–88.
- Hinton, G. E. (1981). A parallel computation that assigns canonical object-based frames of reference. In *Proceedings of the 7th international joint conference on Artificial intelligence- Volume 2*, pages 683–685. Morgan Kaufmann Publishers Inc.
- Hinton, G. E. (1990). Mapping part-whole hierarchies into connectionist networks. *Artificial Intelligence*, 46(1-2):47–75.
- Hitchcock, F. L. (1927). The expression of a tensor or a polyadic as a sum of products. *Journal of Mathematics and Physics*, 6(1-4):164–189.
- Hopfield, J. J. (1982). Neural networks and physical systems with emergent collective computational abilities. *Proceedings of the national academy of sciences*, 79(8):2554–2558.
- Hopfield, J. J. (1984). Neurons with graded response have collective computational properties like those of two-state neurons. *Proceedings of the national academy of sciences*, 81(10):3088–3092.
- Huang, J. and Hagiwara, M. (1999). A new multidimensional associative memory based on distributed representation and its applications. In *IEEE International Conference on Systems, Man, and Cybernetics*, volume 1, pages 194–199.
- Joshi, A., Halseth, J. T., and Kanerva, P. (2016). Language geometry using random indexing. In *International Symposium on Quantum Interaction*, page 265–274. Springer.
- Kanerva, P. (1996). Binary spatter-coding of ordered k-tuples. In *International Conference on Artificial Neural Networks*, pages 869–873.
- Kanerva, P. (1998). Large patterns make great symbols: An example of learning from example. In *International Workshop on Hybrid Neural Systems*, pages 194–203. Springer.
- Kanerva, P. (2009). Hyperdimensional computing: An introduction to computing in distributed representation with high-dimensional random vectors. *Cognitive Computation*, 1(2):139–159.
- Kent, S. J. and Olshausen, B. A. (2017). A vector symbolic approach to scene transformation. In *Cognitive computational neuroscience (CCN '17) (extended abstract) [link]*.
- Kersten, D., Mamassian, P., and Yuille, A. (2004). Object perception as bayesian inference. *Annu. Rev. Psychol.*, 55:271–304.
- Kobayashi, M., Hattori, M., and Yamazaki, H. (2002). Multidirectional associative memory with a hidden layer. *Systems and Computers in Japan*, 33(3):1494–1502.

- Kolda, T. G. and Bader, B. W. (2009). Tensor decompositions and applications. *SIAM review*, 51(3):455–500.
- Kosko, B. (1988). Bidirectional associative memories. *IEEE Transactions on Systems, man, and Cybernetics*, 18(1):49–60.
- Kruskal, J. B. (1977). Three-way arrays: rank and uniqueness of trilinear decompositions, with application to arithmetic complexity and statistics. *Linear algebra and its applications*, 18(2):95–138.
- Lee, D. D. and Seung, H. S. (2001). Algorithms for non-negative matrix factorization. In *Advances in neural information processing systems*, pages 556–562.
- Liu, X. and Sidiropoulos, N. D. (2001). Cramér-rao lower bounds for low-rank decomposition of multidimensional arrays. *IEEE Transactions on Signal Processing*, 49(9):2074–2086.
- Memisevic, R. and Hinton, G. E. (2010). Learning to represent spatial transformations with factored higher-order boltzmann machines. *Neural computation*, 22(6):1473–1492.
- Mumford, D. and Desolneux, A. (2010). *Pattern theory: the stochastic analysis of real-world signals*. AK Peters/CRC Press.
- Nickel, M., Rosasco, L., and Poggio, T. (2016). Holographic embeddings of knowledge graphs. In *Proceedings of the Thirtieth AAAI Conference on Artificial Intelligence*, AAAI’16, pages 1955–1961. AAAI Press.
- Olshausen, B. A., Anderson, C. H., and Van Essen, D. C. (1993). A neurobiological model of visual attention and invariant pattern recognition based on dynamic routing of information. *Journal of Neuroscience*, 13(11):4700–4719.
- Personnaz, L., Guyon, I., and Dreyfus, G. (1986). Collective computational properties of neural networks: New learning mechanisms. *Physical Review A*, 34(5):4217.
- Plate, T. A. (1991). Holographic reduced representations: Convolution algebra for compositional distributed representations. In *International Joint Conference on Artificial Intelligence*, pages 30–35.
- Plate, T. A. (1995). Holographic reduced representations. *IEEE Transactions on Neural Networks*, 6(3):623–641.
- Plate, T. A. (2003). *Holographic reduced representation: Distributed representation of cognitive structure*. CSLI Publications, Stanford, CA.
- Rahimi, A., Datta, S., Kleyko, D., Frady, E. P., Olshausen, B., Kanerva, P., and Rabaey, J. M. (2017). High-dimensional computing as a nanoscalable paradigm. *IEEE Transactions on Circuits and Systems I: Regular Papers*, 64(9):2508–2521.
- Rahimi, A., Kanerva, P., Benini, L., and Rabaey, J. M. (2018). Efficient biosignal processing using hyperdimensional computing: Network templates for combined learning and classification of exg signals. *Proceedings of the IEEE*, 107(1):123–143.

- Raven, J. et al. (2003). Raven progressive matrices. In *Handbook of nonverbal assessment*, pages 223–237. Springer.
- Rosenblatt, F. (1962). *Principles of neurodynamics: Perceptrons and the theory of brain mechanisms*. Spartan Books, Washington, D.C.
- Sidiropoulos, N. D. and Bro, R. (2000). On the uniqueness of multilinear decomposition of n-way arrays. *Journal of Chemometrics: A Journal of the Chemometrics Society*, 14(3):229–239.
- Smolensky, P. (1990). Tensor product variable binding and the representation of symbolic structures in connectionist systems. *Artificial Intelligence*, 46(1-2):159–216.
- Tenenbaum, J. B. and Freeman, W. T. (2000). Separating style and content with bilinear models. *Neural computation*, 12(6):1247–1283.
- Touretzky, D. S. (1990). Boltzcons: Dynamic symbol structures in a connectionist network. *Artificial Intelligence*, 46(1-2):5–46.
- Tucker, L. R. (1963). Implications of factor analysis of three-way matrices for measurement of change. In Harris, C. W., editor, *Problems in measuring change*, pages 122–137. University of Wisconsin Press, Madison WI.
- Tucker, L. R. (1966). Some mathematical notes on three-mode factor analysis. *Psychometrika*, 31(3):279–311.
- Van Vreeswijk, C. and Sompolinsky, H. (1996). Chaos in neuronal networks with balanced excitatory and inhibitory activity. *Science*, 274(5293):1724–1726.
- Vasilescu, M. A. O. and Terzopoulos, D. (2002). Multilinear analysis of image ensembles: Tensorfaces. In *European Conference on Computer Vision*, pages 447–460. Springer.

Appendices

A Tensor Decompositions and Alternating Least Squares

Tensors are multidimensional arrays that generalize vectors and matrices. An F th-order tensor has elements that can be indexed by F separate indexes – a vector is a tensor of order 1 and a matrix is a tensor of order 2. As devices for measuring multivariate time series (for instance video data and shopping preferences) have become more prevalent, the study of tensor decomposition has grown as a subfield of applied mathematics due to the fact that much of this data can be modeled as a tensor. Hitchcock (Hitchcock, 1927) is often credited with originally formulating tensor decompositions, but modern tensor decomposition was popularized in the field of psychometrics by the work of Tucker (Tucker, 1966), Carroll and Chang (Carroll and Chang, 1970), and Harshman (Harshman, 1970).

The type of tensor decomposition that can be most closely related to our factorization problem (given in equation (1)) decomposes an F th-order tensor \mathcal{C} into a sum of tensors each generated by the outer product of F vectors:

$$\mathcal{C} = \sum_{r=1}^R \mathbf{x}_r^{(1)} \circ \mathbf{x}_r^{(2)} \circ \dots \circ \mathbf{x}_r^{(F)} \quad (34)$$

The symbol \circ denotes the outer product $(\mathbf{w} \circ \mathbf{x} \circ \mathbf{y} \circ \mathbf{z})_{ijkl} = w_i x_j y_k z_l$. The interpretation is that each term in the sum is a “rank-one” tensor of order F and that \mathcal{C} can be generated from the sum of R of these rank-one tensors. We say that \mathcal{C} is “rank- R ”. This particular decomposition has at least three different names in the literature - they are Canonical Polyadic Decomposition, coined by Hitchcock, CANonical DECOMPosition (CANDECOMP), coined by Carroll and Chang, and PARAllel FACtor analysis (PARAFAC), coined by Harshman. We will simply call this the CP decomposition, in accordance with the convention used by Kolda (Kolda and Bader, 2009) and many others. CP decomposition makes no mention of a codebook of vectors, such as we had in (1). The search is apparently over all of the vectors in a real-valued vector space. One very useful fact about CP decomposition is that under relatively mild conditions, *if a CP decomposition exists, it is unique* up to a scaling and permutation indeterminacy. Without going into the details, a result in Kruskal (1977) and extended by Sidiropoulos and Bro (2000) gives a sufficient condition for uniqueness of the CP decomposition:

$$\sum_{f=1}^F k_{\mathbf{X}_f} \geq 2R + (F - 1) \quad (35)$$

Where \mathbf{X}_f is a matrix with each column containing the vectors $\mathbf{x}_r^{(f)}$. The scalar $k_{\mathbf{X}_f}$ is the Kruskal rank of the matrix \mathbf{X}_f , defined as the maximum value k such that any k columns of \mathbf{X}_f are linearly independent (Kruskal, 1977). There is a necessary condition for uniqueness of the CP decomposition due to Liu and Sidiropoulos (2001), but it is relatively weak and we will not cover it here.

One can *almost* fit the factorization problem (1) into the framework of CP decomposition by taking the rank R of the CP decomposition to be 1 and restricting the vectors to be

bipolar. However, this creates a tensor of order F whereas (1) involves factoring the vector given by the diagonal of this tensor. We’ve already run into one major problem regarding the uniqueness of the decomposition: with $R = 1$, the Kruskal rank of each matrix \mathbf{X}_f will be 1, meaning the sufficient condition for uniqueness of the CP decomposition cannot be satisfied. Additionally, the *Hadamard* product means (1) technically differs from CP decomposition, and it makes the uniqueness issue worse still, because the target \mathcal{C} is no longer an F -order tensor but rather just a vector, with many fewer degrees of freedom. The uniqueness issue can be remedied by searching over a discrete set of vectors \mathbb{X}_f for each factor, such that the factorization of \mathbf{c} with respect to these vectors is unique. The CANonical DEcomposition with LINear Constraints (CANDELINC) decomposition (Carroll et al., 1980) is essentially CP decomposition with the additional requirement that $\mathbf{x}_r^{(f)} = \mathbf{X}_f \mathbf{a}_{f,r}$. It should be clear that by placing the bipolar vectors of \mathbb{X}_f into the columns of \mathbf{X}_f and taking $R = 1$, we have something very close to (1), the only remaining difference being between the Hadamard product for (1) and the outer product for CANDELINC. The fact that the object to be factored is an N -dimensional vector as opposed to an $N \times N \times \dots N$ -dimensional tensor would seem to make the problem significantly harder – there is much less information about the underlying factors present in the composite object.

Another popular tensor decomposition is known as the Tucker Decomposition (Tucker, 1963, 1966). It adds to CP decomposition an order- F “core tensor” \mathcal{G} that modifies the interaction between each of the factors:

$$\mathcal{C} = \sum_{p=1}^P \sum_{q=1}^Q \dots \sum_{r=1}^R g_{pq\dots r} \mathbf{x}_p^{(1)} \circ \mathbf{x}_q^{(2)} \circ \dots \circ \mathbf{x}_r^{(F)} \quad (36)$$

This adds many more parameters compared to CP decomposition, which is a special case of Tucker decomposition when \mathcal{G} is the identity. For the purpose of illustration, we reprint in Figure 16 (with a slight relabeling) a figure from the excellent review by Kolda and Bader (Kolda and Bader, 2009) that depicts an order-3 Tucker decomposition. This decomposition

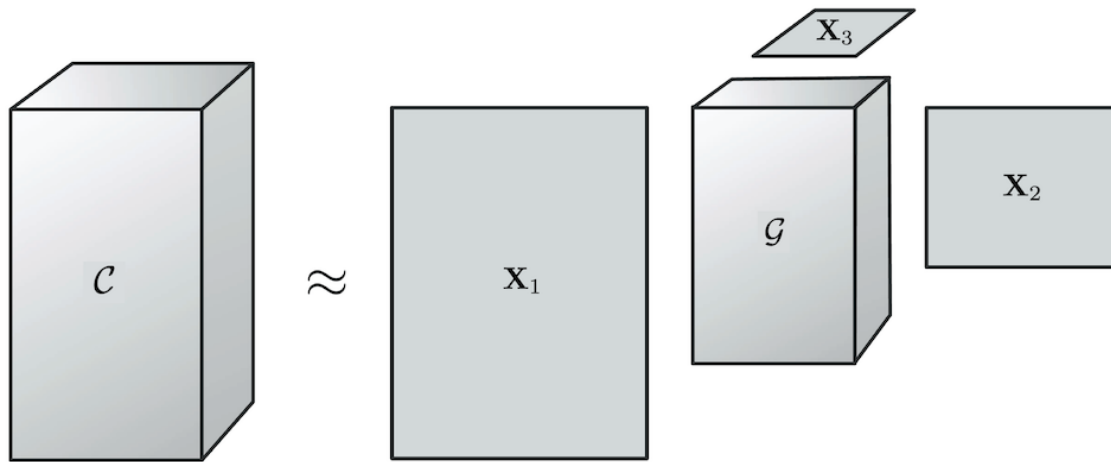


Figure 16: Tucker decomposition with 3 factors

goes by many other names, most popularly the Higher-order SVD, coined in De Lathauwer et al. (2000). The Tucker decomposition can be found via Alternating Least Squares (see Kolda and Bader (2009), Section 4.2, for a tutorial), although the problem is somewhat harder than CP decomposition, both by being computationally more expensive and by being non-unique. Despite this fact, the applications of Tucker decomposition are wide-ranging – it has been used in psychometrics, signal processing, and computer vision. One well-known application of Tucker decomposition in computer vision was TensorFaces (Vasilescu and Terzopoulos, 2002). This model was able to factorize identity, illumination, viewpoint, and facial expression in a dataset consisting of face images.

The first algorithm we introduced in Section 2.3 of the main text was Alternating Least Squares (ALS) and we applied it to our *vector factorization* problem. Alternating Least Squares is actually most well-known for finding tensor decompositions, particularly the CP and Tucker decomposition. For CP decomposition, ALS updates can be expressed in terms of a normal matrix product and an operation called the Khatri-Rao product – see Kolda and Bader (2009), specifically Section 3.4 for more detail. This technique is relatively efficient, easy to understand, and works well in practice.

When applied to the vector factorization problem, Alternating Least Squares has dynamics given by equation (8). We start with $\mathbf{a}_f[0] = \mathbf{1}$, giving equal initial weight to each of the codevectors. These updates always either reduce the squared error loss or leave it unchanged, which, due to the lower-boundedness of this function, implies that Alternating Least Squares will converge to a local minimum of the squared error. We found that Alternating Least Squares was not competitive with Resonator Circuits and its failure mode was getting stuck in suboptimal local minima of the squared error. Despite the fact that it is effective for finding CP decompositions of tensors, Alternating Least Squares is apparently not the right algorithm for solving (1).

B General notes on gradient-based algorithms

When \mathcal{L} is the negative inner product, the gradient with respect to \mathbf{a}_f is:

$$\begin{aligned}\nabla_{\mathbf{a}_f} \mathcal{L} &= -\mathbf{X}_f^T (\mathbf{c} \odot \hat{\mathbf{x}}^{(1)} \odot \dots \odot \hat{\mathbf{x}}^{(f-1)} \odot \hat{\mathbf{x}}^{(f+1)} \odot \dots \odot \hat{\mathbf{x}}^{(F)}) \\ &= -\mathbf{X}_f^T (\mathbf{c} \odot \hat{\mathbf{o}}^{(f)})\end{aligned}\tag{37}$$

The term $\mathbf{c} \odot \hat{\mathbf{o}}^{(f)}$ can be interpreted as an estimate for what $\hat{\mathbf{x}}^{(f)}$ should be based on the current estimates for the *other* factors. Multiplying by \mathbf{X}_f^T compares the similarity of this vector to each of the candidate codevectors we are entertaining, with the smallest element of $\nabla_{\mathbf{a}_f} \mathcal{L}$ (its value is likely to be negative with large absolute value) indicating the codevector which matches best. Following the negative gradient will cause this coefficient to increase more than the coefficients corresponding to the other codevectors. When \mathcal{L} is the squared error, the gradient with respect to \mathbf{a}_f is:

$$\begin{aligned}\nabla_{\mathbf{a}_f} \mathcal{L} &= \mathbf{X}_f^T \left((\mathbf{c} - \hat{\mathbf{x}}^{(1)} \odot \dots \odot \hat{\mathbf{x}}^{(F)}) \odot (-\hat{\mathbf{x}}^{(1)} \odot \dots \odot \hat{\mathbf{x}}^{(f-1)} \odot \hat{\mathbf{x}}^{(f+1)} \odot \dots \odot \hat{\mathbf{x}}^{(F)}) \right) \\ &:= \mathbf{X}_f^T \left(\hat{\mathbf{x}}^{(f)} \odot (\hat{\mathbf{o}}^{(f)})^2 - \mathbf{c} \odot \hat{\mathbf{o}}^{(f)} \right)\end{aligned}\tag{38}$$

This looks somewhat similar to the gradient for the negative inner product – they differ by an additive term given by $\mathbf{X}_f^T \left(\hat{\mathbf{x}}^{(f)} \odot (\hat{\mathbf{o}}^{(f)})^2 \right)$. At the vertices of the hypercube all the elements of $\hat{\mathbf{x}}^{(f)}$ are 1 or -1 and the term $(\hat{\mathbf{o}}^{(f)})^2$ disappears, making the difference between the two gradients just $\mathbf{X}_f^T \hat{\mathbf{x}}^{(f)}$. Among other things, this makes the gradient of the squared error equal to zero at the global minimizer $\mathbf{x}_\star^{(1)} \dots \mathbf{x}_\star^{(F)}$, which is not the case with the negative inner product. To be clear, (37) is the gradient when the loss function is the negative inner product, while (38) is the gradient when the loss function is the squared error.

B.1 Fixed-stepsize gradient descent on the squared error

In fixed-step-size gradient descent for unconstrained convex optimization problems, one must often add a restriction on the stepsize, related to the *smoothness* of the loss function, in order to ensure that the iterates converge to a fixed point. We say that a function \mathcal{L} is L -smooth when its gradient is Lipschitz continuous with constant L :

$$\|\nabla \mathcal{L}(\mathbf{x}) - \nabla \mathcal{L}(\mathbf{y})\|_2 \leq L \|\mathbf{x} - \mathbf{y}\|_2 \quad \forall \mathbf{x}, \mathbf{y} \quad (39)$$

For a function that is twice-differentiable, this is equivalent to the condition

$$\mathbf{0} \preceq \nabla^2 \mathcal{L}(\mathbf{x}) \preceq L \mathbf{I} \quad \forall \mathbf{x} \quad (40)$$

Where $\mathbf{0}$ is the matrix of all zeros and \mathbf{I} is the identity. Absent some procedure for adjusting the stepsize η at each iteration to account for the degree of local smoothness, or some additional assumption we place on the loss to make sure that it is sufficiently smooth, we should be wary that convergence may not be guaranteed. On our factorization problem we find this to be an issue. Unconstrained gradient descent on the squared error works for the simplest problems, where M is small and the factorization can be easily found by any of the algorithms in this paper. However, as M increases, the exceedingly “sharp” landscape of the squared error loss makes the iterates very sensitive to the step size η , and the components of $\mathbf{a}_f[t]$ can become very large. When this happens, the term $\hat{\mathbf{o}}^{(f)}[t]$ amplifies this problem (it multiplies all but one of the $\mathbf{a}_f[t]$ ’s together) and causes numerical instability issues. With the squared error loss, the smoothness is very poor: we found that fixed-stepsize gradient descent on the squared error was so sensitive to η that it made the method practically useless for solving the factorization problem. Iterative Soft Thresholding and Fast Iterative Soft Thresholding use a dynamic step size to avoid this issue (see equation (41)). In contrast, the negative inner product loss, with respect to each factor, is in some sense *perfectly smooth* (it is linear), so the step size does not factor into convergence proofs.

C Iterative Soft Thresholding (ISTA) and Fast Iterative Soft Thresholding (FISTA)

Iterative Soft Thresholding is a type of *proximal gradient descent*. The proximal operator for any convex function $h(\cdot)$ is defined as

$$\text{prox}_h(\mathbf{x}) := \arg \min_{\mathbf{z}} \frac{1}{2} \|\mathbf{z} - \mathbf{x}\|_2^2 + h(\mathbf{z})$$

When $h(\mathbf{z})$ is $\lambda\|\mathbf{z}\|_1$, the proximal operator is the so-called ‘‘soft-thresholding’’ function which we denote by \mathcal{S} :

$$(\mathcal{S}[\mathbf{x}; \gamma])_i := \text{sgn}(x_i) \max(|x_i| - \gamma, 0)$$

Consider taking the squared error loss and adding to it $\lambda\|\mathbf{a}_f\|_1$:

$$\mathcal{L}(\mathbf{c}, \hat{\mathbf{c}}) + \lambda\|\mathbf{a}_f\|_1 = \frac{1}{2}\|\mathbf{c} - \hat{\mathbf{c}}\|_2^2 + \lambda\|\mathbf{a}_f\|_1$$

Applying soft thresholding clearly minimizes this augmented loss function. The strategy is to take gradient steps with respect to the squared error loss but then to pass those updates through the soft thresholding function \mathcal{S} . This flavor of proximal gradient descent, where $\hat{\mathbf{c}}$ is a linear function of \mathbf{a}_f and $h(\cdot)$ is the ℓ_1 norm, is called the Iterative Soft Thresholding Algorithm (Daubechies et al., 2004), and is a somewhat old and popular approach for finding sparse solutions to large-scale linear inverse problems.

The dynamics of ISTA are given in equation (9) and there are a few parameters worth discussing. First, the dynamic stepsize η can be set via backtracking line search or, as we did, by computing the Lipschitz constant of the function gradient:

$$\eta = \frac{1}{L} \quad | \quad \|\nabla_{\mathbf{a}}\mathcal{L}(\mathbf{x}) - \nabla_{\mathbf{a}}\mathcal{L}(\mathbf{y})\|_2 \leq L\|\mathbf{x} - \mathbf{y}\|_2 \quad \forall \mathbf{x}, \mathbf{y} \quad (41)$$

The scalar λ is a hyperparameter that effectively sets the sparsity of the solutions considered – its value should be tuned in order to get good performance in practice. In the experiments we show in this paper λ was 0.01. The initial state $\mathbf{a}_f[0]$ is set to $\mathbf{1}$.

Convergence analysis of ISTA is beyond the scope of this paper, but it has been shown in various places (Bredies and Lorenz (2008), for instance) that ISTA will converge at a rate $\simeq \mathcal{O}(1/t)$. Iterative Soft Thresholding works well in practice, although for 4 or more factors we find that it is not quite as effective as the algorithms that do constrained descent on the negative inner product loss. By virtue of not directly constraining the coefficients, ISTA allows them to grow outside of $[0, 1]^N$. This may make it easier to find the minimizers $\mathbf{a}_1^*, \mathbf{a}_2^*, \dots, \mathbf{a}_F^*$, but it may also lead the method to encounter more suboptimal local minimizers, which we found to be the case in practice.

One common criticism of ISTA is that it can get trapped in shallow parts of the loss surface and thus suffers from slow convergence (Bredies and Lorenz, 2008). A straightforward improvement, based on Nesterov’s momentum for accelerating first-order methods, was proposed by Beck and Teboulle (2009), which they call Fast Iterative Soft Thresholding (FISTA). The dynamics of FISTA are written in equation (10), and converge at the significantly better rate of $\simeq \mathcal{O}(1/t^2)$, a result proven in Beck and Teboulle (2009). Despite this difference in *worst-case* convergence rate, we find that the average-case convergence rate on our particular factorization problem does not significantly differ. Initial coefficients $\mathbf{a}_f[0]$ are set to $\mathbf{1}$ and auxiliary variable α_t is initialized to 1. For all experiments λ was set the same as for ISTA, to 0.01.

D Projected Gradient Descent

Starting from the general optimization form of the factorization problem (5), what kind of constraint might it be reasonable to enforce on \mathbf{a}_f ? The most obvious is that \mathbf{a}_f lie on

the simplex $\Delta_{M_f} := \{\mathbf{x} \in \mathbb{R}^{M_f} \mid \sum_i x_i = 1, x_i \geq 0 \forall i\}$. Enforcing this constraint means that $\hat{\mathbf{x}}^{(f)}$ stays within the $-1, 1$ hypercube at all times and, as we noted, the optimal values $\mathbf{a}_1^*, \mathbf{a}_2^*, \dots, \mathbf{a}_F^*$ happen to lie at vertices of the simplex, the standard basis vectors \mathbf{e}_i . Another constraint set worth considering is the ℓ_1 ball $\mathcal{B}_{\|\cdot\|_1}[1] := \{\mathbf{x} \in \mathbb{R}^{M_f} \mid \|\mathbf{x}\|_1 \leq 1\}$. This set contains the simplex, but it encompasses much more of \mathbb{R}^{M_f} . One reason to consider the ℓ_1 ball is that it dramatically increases the number of feasible global optimizers of (5), from which we can easily recover the specific solution to (1). This is due to the fact that:

$$c = \mathbf{X}_1 \mathbf{a}_1^* \odot \mathbf{X}_2 \mathbf{a}_2^* \odot \dots \odot \mathbf{X}_F \mathbf{a}_F^* \iff c = \mathbf{X}_1(-\mathbf{a}_1^*) \odot \mathbf{X}_2(-\mathbf{a}_2^*) \odot \dots \odot \mathbf{X}_F \mathbf{a}_F^*$$

and moreover any number of distinct pairs of factor coefficients can be made negative – this sign change cancels out. The result is that while the simplex constraint only allows solution $\mathbf{a}_1^*, \mathbf{a}_2^*, \dots, \mathbf{a}_F^*$, the ℓ_1 ball constraint also allows solutions $-\mathbf{a}_1^*, -\mathbf{a}_2^*, \mathbf{a}_3^*, \dots, \mathbf{a}_F^*$, and $\mathbf{a}_1^*, \mathbf{a}_2^*, -\mathbf{a}_3^*, \dots, -\mathbf{a}_F^*$, and $-\mathbf{a}_1^*, -\mathbf{a}_2^*, -\mathbf{a}_3^*, \dots, -\mathbf{a}_F^*$, etc. These spurious global minimizers can easily be detected by checking the sign of the largest-magnitude component of \mathbf{a}_f . If it is negative we can then multiply by -1 to get \mathbf{a}_f^* . Choosing the ℓ_1 ball over the simplex is purely motivated from the perspective that increasing the size of the constraint set may make finding the global optimizers easier. However, we found that in practice, it did not significantly matter whether Δ_{M_f} or $\mathcal{B}_{\|\cdot\|_1}[1]$ was used to constrain \mathbf{a}_f .

There exist algorithms for efficiently computing projections onto both the simplex and the ℓ_1 ball (see Held et al. (1974), Duchi et al. (2008), and Condat (2016)). We use a variant summarized in Duchi et al. (2008) that has computational complexity $\mathcal{O}(M_f \log M_f)$ – recall that \mathbf{a}_f has M_f components, so this is the dimensionality of the simplex or the ℓ_1 ball being projected onto. When constraining to the simplex, we set the initial coefficients $\mathbf{a}_f[0]$ to $\frac{1}{M_f} \mathbf{1}$, the center of the simplex. When constraining to the unit ℓ_1 ball we set $\mathbf{a}_f[0]$ to $\frac{1}{2M_f} \mathbf{1}$, so that all coefficients are equal but the vector is on the interior of the ball. The only hyperparameter is η , which, in all experiments was set to 0.01.

Taking projected gradient steps on the negative inner product loss works well and is guaranteed to converge, whether we use the simplex or the ℓ_1 ball constraint. Convergence is guaranteed due to this intuitive fact: any part of $-\eta \nabla_{\mathbf{a}_f} \mathcal{L}$ not in $\mathcal{N}(\mathcal{P}_{C_f}[\mathbf{x}])$, induces a change in \mathbf{a}_f , denoted by $\Delta \mathbf{a}_f[t]$ which must make an acute angle with $-\nabla_{\mathbf{a}_f} \mathcal{L}$. This is by *the definition of orthogonal projection*, and it is a sufficient condition for showing that $\Delta \mathbf{a}_f[t]$ decreases the value of the loss function. Projected Gradient Descent iterates always reduce the value of the negative inner product loss or leave it unchanged; the function is bounded below on the simplex and the ℓ_1 ball, so this algorithm is guaranteed to converge.

Applying projected gradient descent on the squared error did not work, which is related to the smoothness issue we discussed in Appendix B.1, although the behavior was not as dramatic as with unconstrained gradient descent. We observed in practice that projected gradient descent on the squared error loss easily falls into limit cycles of the dynamics. It was for this reason that we restricted our attention with projected gradient descent to the negative inner product loss.

E Multiplicative Weights

When we have simplex constraints $C_f = \Delta_{M_f}$, the Multiplicative Weights algorithm is an elegant way to perform the superposition search. It naturally enforces the simplex constraint by maintaining a set of auxiliary variables, the ‘weights’, which define the choice of \mathbf{a}_f at each iteration. See equation (12) for the dynamics of Multiplicative Weights. We choose a fixed stepsize $\eta \leq 0.5$ and initial values for the weights all one: $\mathbf{w}_f[0] = \mathbf{1}$. In experiments in this paper we set $\eta = 0.3$. The variable ρ exists to normalize the term $\frac{1}{\rho} \nabla_{\mathbf{a}_f} \mathcal{L}$ so that each element lies in the interval $[-1, 1]$.

Here we *briefly* discuss the motivation and history of the Multiplicative Weights algorithm. Curious readers are referred to the survey of Arora et al. (2012) for more detail. The terminology we use below is inherited from online optimization and game theory where problems are often conceptualized as a decision maker playing a game and where the decision maker wants to choose actions in the game that are optimal in some sense. Suppose this decision maker is playing a game where at each iteration t they choose one of K possible actions, for which they suffer some kind of cost $m_k[t]$ where k is the action they chose. A fixed decision policy chooses the same action at each iteration. After T iterations, among the fixed decision policies, there is one which gives the lowest total cost, sometimes called the ‘best expert’:

$$k^* := \arg \min_k \sum_{t=1}^T m_k[t]$$

The difference between the cumulative cost of any particular policy and the cost of the best expert is called the regret R_T of that policy. It can be shown that Multiplicative Weights yields a regret which is bounded above by $\frac{\ln k}{\eta} + \eta T$ where η is a stepsize used to update the weights, analogously to what we have written in (12). Dividing by T and taking it to ∞ , we see that, by running the game for enough steps, the time-averaged regret of Multiplicative Weights is no worse than the (arbitrarily small) constant η . That is, it yields a decision policy which has average cost no more than η worse than the ‘best expert’. What is truly remarkable about Multiplicative Weights is that this result holds for any arbitrary costs $m_k[t]$ as long as they are bounded (hence the role for ρ in (12)), including when the costs are chosen in an *adversarial* way to try and fool the decision policy into making incorrect choices.

Through a straightforward generalization of the discrete actions into directions in a continuous vector space, one can apply Multiplicative Weights to problems of *online convex optimization*, which is discussed at length in Arora et al. (2012) and Hazan et al. (2016). The cost $m_k[t]$ from the development above is precisely the k th element of $\frac{1}{\rho} \nabla f$, where f is a convex loss function – in the online convex optimization setting, the costs are given by the normalized gradient of the loss function. We can think of solving our problem (5) as if it were an online convex optimization problem where we update each factor $\hat{\mathbf{x}}^{(f)}$ according to its own Multiplicative Weights update, one at a time. The function \mathcal{L} is convex with respect to \mathbf{a}_f , but is changing at each iteration due the updates for the *other* factors - it is in this sense the the we are treating (5) as an *online* convex optimization problem.

E.1 Multiplicative Weights is a descent method

A descent method on \mathcal{L} is any algorithm that iterates $\mathbf{a}_f[t+1] = \mathbf{a}_f[t] + \eta[t]\Delta\mathbf{a}_f[t]$ where the update $\Delta\mathbf{a}_f[t]$ makes an acute angle with $-\nabla_{\mathbf{a}_f}\mathcal{L}$: $\nabla_{\mathbf{a}_f}\mathcal{L}^T\Delta\mathbf{a}_f[t] < 0$. In the case of Multiplicative Weights, we can equivalently define a descent method based on $\nabla_{\mathbf{w}_f}\bar{\mathcal{L}}^T\Delta\mathbf{w}_f[t] < 0$ where $\bar{\mathcal{L}}(\mathbf{w}_f)$ is the loss as a function of the *weights* and $\nabla_{\mathbf{w}_f}\bar{\mathcal{L}}$ is its gradient with respect to those weights. The loss as a function of the weights comes via the substitution $\mathbf{a}_f = \frac{\mathbf{w}_f}{\sum_i w_{fi}} := \frac{\mathbf{w}_f}{\Phi_f}$. We now prove that $\nabla_{\mathbf{w}_f}\bar{\mathcal{L}}^T\Delta\mathbf{w}_f[t] < 0$:

$$\begin{aligned}
\nabla_{\mathbf{w}_f}\bar{\mathcal{L}} &= \frac{\partial\mathbf{a}_f}{\partial\mathbf{w}_f} \frac{\partial\mathcal{L}}{\partial\mathbf{a}_f} \\
&= \begin{bmatrix} \frac{\Phi_f - w_{f1}}{\Phi_f^2} & \frac{-w_{f2}}{\Phi_f^2} & \dots & \frac{-w_{fk}}{\Phi_f^2} \\ \frac{-w_{f1}}{\Phi_f^2} & \frac{\Phi_f - w_{f2}}{\Phi_f^2} & \dots & \frac{-w_{fk}}{\Phi_f^2} \\ \vdots & \vdots & \ddots & \vdots \\ \frac{-w_{f1}}{\Phi_f^2} & \frac{-w_{f2}}{\Phi_f^2} & \dots & \frac{\Phi_f - w_{fk}}{\Phi_f^2} \end{bmatrix} \nabla_{\mathbf{a}_f}\mathcal{L} \\
&= \left(\frac{1}{\Phi_f}\mathbf{I} - \frac{1}{\Phi_f^2}\mathbf{1}\mathbf{w}_f^T \right) \nabla_{\mathbf{a}_f}\mathcal{L} \\
&= \frac{1}{\Phi_f}\nabla_{\mathbf{a}_f}\mathcal{L} - \frac{\mathcal{L}(\mathbf{a}_f)}{\Phi_f}\mathbf{1}
\end{aligned} \tag{42}$$

This allows us to write down $\Delta\mathbf{w}_f[t]$ in terms of $\nabla_{\mathbf{w}_f}\bar{\mathcal{L}}$:

$$\begin{aligned}
\Delta\mathbf{w}_f[t] &= -\frac{1}{\rho}\mathbf{w}_f[t] \odot \nabla_{\mathbf{a}_f}\mathcal{L} = -\frac{1}{\rho}\mathbf{w}_f[t] \odot \left(\Phi_f\nabla_{\mathbf{w}_f}\bar{\mathcal{L}} + \mathcal{L}(\mathbf{a}_f[t])\mathbf{1} \right) \\
&= -\frac{\Phi_f}{\rho}\text{diag}(\mathbf{w}_f[t])\nabla_{\mathbf{w}_f}\bar{\mathcal{L}} - \frac{\mathcal{L}(\mathbf{a}_f[t])}{\rho}\mathbf{w}_f[t]
\end{aligned} \tag{43}$$

And then we can easily show the desired result:

$$\begin{aligned}
\nabla_{\mathbf{w}_f}\bar{\mathcal{L}}^T\Delta\mathbf{w}_f[t] &= -\frac{\Phi_f}{\rho}\nabla_{\mathbf{w}_f}\bar{\mathcal{L}}^T\text{diag}(\mathbf{w}_f[t])\nabla_{\mathbf{w}_f}\bar{\mathcal{L}} - \frac{\mathcal{L}(\mathbf{a}_f[t])}{\rho}\nabla_{\mathbf{w}_f}\bar{\mathcal{L}}^T\mathbf{w}_f[t] \\
&= -\frac{\Phi_f}{\rho}\nabla_{\mathbf{w}_f}\bar{\mathcal{L}}^T\text{diag}(\mathbf{w}_f[t])\nabla_{\mathbf{w}_f}\bar{\mathcal{L}} - \frac{\mathcal{L}(\mathbf{a}_f[t])}{\rho}\left(\frac{1}{\Phi_f}\nabla_{\mathbf{a}_f}\mathcal{L}^T - \frac{\mathcal{L}(\mathbf{a}_f[t])}{\Phi_f}\mathbf{1}^T \right)\mathbf{w}_f[t] \\
&= -\frac{\Phi_f}{\rho}\nabla_{\mathbf{w}_f}\bar{\mathcal{L}}^T\text{diag}(\mathbf{w}_f[t])\nabla_{\mathbf{w}_f}\bar{\mathcal{L}} - \frac{\mathcal{L}(\mathbf{a}_f[t])}{\rho}\left(\mathcal{L}(\mathbf{a}_f[t]) - \mathcal{L}(\mathbf{a}_f[t]) \right) \\
&= -\frac{\Phi_f}{\rho}\nabla_{\mathbf{w}_f}\bar{\mathcal{L}}^T\text{diag}(\mathbf{w}_f[t])\nabla_{\mathbf{w}_f}\bar{\mathcal{L}} \\
&< 0
\end{aligned} \tag{44}$$

The last line follows directly from the fact that \mathbf{w}_f are always positive by construction in Multiplicative Weights. Therefore, the matrix $\text{diag}(\mathbf{w}_f[t])$ is positive definite and the term $\frac{\Phi_f}{\rho}$ is strictly greater than 0. We've shown that the iterates of Multiplicative Weights always make steps in descent directions. When the loss \mathcal{L} is the negative inner product, it is

guaranteed to decrease at each iteration. Empirically, multiplicative weights applied to the squared error loss *also always decreases the loss function*. This is likely due to the fact that the stepsize is normalized by ρ at each iteration in Multiplicative Weights, which alleviates the smoothness issue we have mentioned before. Both functions are bounded below over the constraint set Δ_{M_f} , so therefore Multiplicative Weights must converge to a fixed point. In practice, we pick a step size η between 0.1 and 0.5 and run the algorithm until the normalized magnitude of the change in the coefficients is below some small threshold:

$$\frac{\left| \mathbf{a}_f[t+1] - \mathbf{a}_f[t] \right|}{\eta} < \epsilon$$

F Map Seeking Circuits

Map Seeking Circuits (MSCs) are neural networks designed to solve invariant pattern recognition problems. Their theory and applications have been gradually developed by Arathorn and colleagues over the past 18 years (see, for example, Arathorn (2001, 2002), Gedeon and Arathorn (2007), and Harker et al. (2007)), but remain largely unknown outside of a small community of vision researchers. In their original conception, they solve a ‘‘correspondence maximization’’ or ‘‘transformation discovery’’ problem in which the network is given a visually transformed instance of some template object and has to recover the identity of the object as well as a set of transformations that explain its current appearance. The approach taken in Map Seeking Circuits is to superimpose the possible transformations in the same spirit as we have outlined for solving the factorization problem. We cannot give the topic a full treatment here but simply note that the original formulation of Map Seeking Circuits can be directly translated to our factorization problem wherein each type of transformation (e.g. translation, rotation, scale) is one of the F factors, and the particular values of the transformation are vectors in the codebooks $\mathbb{X}_1, \mathbb{X}_2, \dots, \mathbb{X}_F$. The loss function is $\mathcal{L} : \mathbf{x}, \mathbf{y} \mapsto -\langle \mathbf{x}, \mathbf{y} \rangle$ and the constraint set is $[0, 1]^{M_f}$ (both by convention in Map Seeking Circuits). The dynamics of Map Seeking Circuit are given in equation (13), with initial values $\mathbf{a}_f[0] = \mathbf{1}$ for each factor. The small threshold ϵ is a hyperparameter, which we set to 10^{-5} in experiments, along with the stepsize $\eta = 0.1$. Gedeon and Arathorn (2007) and Harker et al. (2007) proved (with some minor technicalities we will not detail here) that Map Seeking Circuits always converge to either a scalar multiple of a canonical basis vector, or the zero vector. That is, $\mathbf{a}_f[\infty] = \beta_f \mathbf{e}_i$ or $\mathbf{0}$ (where $(\mathbf{e}_i)_j = 1$ if $j = i$ and 0 otherwise, and β_f is a positive scalar).

Due to the normalizing term ρ , the updates to \mathbf{a}_f *can never be positive*. Among the components of $\nabla_{\mathbf{a}_f} \mathcal{L}$ which are negative, the one with the largest magnitude corresponds to a component of \mathbf{a}_f which sees an update of 0. All other components are decreased by an amount which is proportional to the gradient. We noted in comments on (37) that the smallest element of $\nabla_{\mathbf{a}_f} \mathcal{L}$ corresponds to the codevector which best matches $\mathbf{c} \odot \hat{\mathbf{o}}^{(f)}$, a ‘‘suggestion’’ for $\hat{\mathbf{x}}^{(f)}$ based on the current states of the other factors. The dynamics of Map Seeking Circuits thus preserves the weight of the codevector which matches best and decreases the weight of the other codevectors, by an amount which is proportional to their own match. Once the weight on a codevector drops below the threshold, it is set to zero and no longer participates in the search. The phenomenon wherein the correct coefficient $a_{f_i^*}$

drops out of the search is called “sustained collusion” by Arathorn (Arathorn, 2002) and is a failure mode of Map Seeking Circuits.

G Percolated noise in Outer Product Resonator Circuits

A Resonator Circuit with outer product weights $\mathbf{X}_f \mathbf{X}_f^T$ that is initialized to the correct factorization is not guaranteed to remain there, just as a Hopfield Network with outer product weights initialized to one of the ‘memories’ is not guaranteed to remain there. This is in contrast to a Resonator Circuit (and a Hopfield Network) with Ordinary Least Squares weights $\mathbf{X}_f (\mathbf{X}_f^T \mathbf{X}_f)^{-1} \mathbf{X}_f^T$, for which each of the codevectors are always fixed points. In this section when we refer simply to a Resonator Circuit or a Hopfield Network we are referring to the variants of these models that use outer product weights. Section G.1 derives equation (19) in the main text, while Sections G.2 and G.3 derive equations (20) - (27).

G.1 First factor

The stability of the first factor in a Resonator Circuit is the same as the stability of the state of a Hopfield network – at issue is the distribution of $\hat{\mathbf{x}}^{(1)}[1]$:

$$\hat{\mathbf{x}}^{(1)}[1] = \text{sgn}(\mathbf{X}_f \mathbf{X}_f^T \mathbf{x}_\star^{(1)}) := \text{sgn}(\mathbf{\Gamma})$$

Assuming each codevector (each column of \mathbf{X}_f) is a random bipolar vector, each component of $\mathbf{\Gamma}$ is a random variable. Its distribution can be deduced from writing it out in terms of constant and random components:

$$\begin{aligned} \Gamma_i &= \sum_m^{M_1} \sum_j^N (\mathbf{x}_m^{(1)})_i (\mathbf{x}_m^{(1)})_j (\mathbf{x}_\star^{(1)})_j \\ &= N (\mathbf{x}_\star^{(1)})_i + \sum_{m \neq \star}^{M_1} \sum_j^N (\mathbf{x}_m^{(1)})_i (\mathbf{x}_m^{(1)})_j (\mathbf{x}_\star^{(1)})_j \\ &= N (\mathbf{x}_\star^{(1)})_i + (M_1 - 1) (\mathbf{x}_\star^{(1)})_i + \sum_{m \neq \star}^{M_1} \sum_{j \neq i}^N (\mathbf{x}_m^{(1)})_i (\mathbf{x}_m^{(1)})_j (\mathbf{x}_\star^{(1)})_j \end{aligned} \quad (45)$$

The third term is a sum of $(N - 1)(M_1 - 1)$ i.i.d. Rademacher random variables, which in the limit of large NM_1 can be well-approximated by a Gaussian random variable with mean zero and variance $(N - 1)(M_1 - 1)$. Therefore, Γ_i is approximately Gaussian with mean $(N + M_1 - 1) (\mathbf{x}_\star^{(1)})_i$ and variance $(N - 1)(M_1 - 1)$. The probability that $(\hat{\mathbf{x}}^{(1)}[1])_i \neq (\mathbf{x}_\star^{(1)})_i$ is given by the cumulative density function of the Normal distribution:

$$\begin{aligned} h_1 &:= Pr [(\hat{\mathbf{x}}^{(1)}[1])_i \neq (\mathbf{x}_\star^{(1)})_i] \\ &= \Phi \left(\frac{-N - M_1 + 1}{\sqrt{(N - 1)(M_1 - 1)}} \right) \end{aligned} \quad (46)$$

We care about the ratio M_1 / N and how the bitflip probability h_1 scales with this number. We’ve called this h_1 to denote the Hopfield bitflip probability but it’s also r_1 , the bitflip

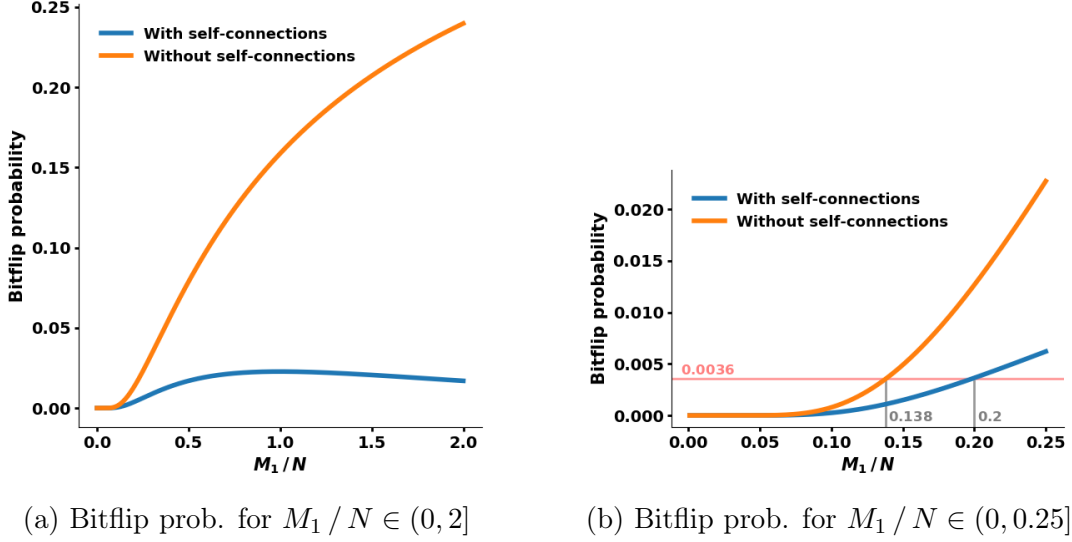


Figure 17: Effect of self-connections on bitflip probability

probability for the *first* factor of a Resonator Circuit. We’ll see that for the second, third, fourth, and other factors, h_f will not equal r_f , which is what we mean by percolated noise, the focus of Section 4.1 in the main text. If we eliminate all “self-connection” terms from $\mathbf{X}_f \mathbf{X}_f^T$, by setting each element on the diagonal to zero, then the second term in (45) is eliminated and the bitflip probability is $\Phi\left(\frac{-N}{\sqrt{(N-1)(M_1-1)}}\right)$. This is actually significantly different from (46), which we can see in Figure 17. With self-connections, the bitflip probability is maximized when $M_1 = N$ (the reader can verify this via simple algebra), and its maximum value is ≈ 0.023 . Without self-connections, the bitflip probability asymptotes at 0.5. The actual useful operating regime of both these networks is where M_1 is significantly less than N , which we zoom in on in Figure 17b. A “mean-field” analysis of Hopfield Networks developed by Amit, Gutfreund, and Sompolinsky (Amit et al., 1985, 1987) showed that when $M_1/N > 0.138$, a phase-change phenomenon occurs in which a small number of initial bitflips (when the probability is 0.0036 according to the above approximation) build up over subsequent iterations and the network almost always moves far away from $\mathbf{x}_\star^{(1)}$, making it essentially useless. We can see that the same bitflip probability is suffered at a significantly higher value for M_1/N when we have self-connections – the vector $\mathbf{x}_\star^{(1)}$ is significantly more stable in this sense. We also found that a Resonator Circuit has higher operational capacity (see Section 4.2) when we leave in the self-connections. As a third point of interest, computing $\mathbf{X}_f \mathbf{X}_f^T \mathbf{x}_\star^{(1)}$ is often much faster when we keep each codebook matrix separate (instead of forming the synaptic matrix $\mathbf{X}_f \mathbf{X}_f^T$ directly), in which case removing the self-connection terms involves extra computation in each iteration of the algorithm. For all of these reasons, we choose to keep self-connection terms in the Resonating Circuit. It is probably worth noting that in some places the specification of a Hopfield Network has included a “bias” term which serves an equivalent role as retaining the self-connections in the weight matrix.

G.2 Second factor

When we update the second factor, we have

$$\hat{\mathbf{x}}^{(2)}[1] = \text{sgn}\left(\mathbf{X}_f \mathbf{X}_f^T (\hat{\boldsymbol{\delta}}^{(2)}[1] \odot \mathbf{c})\right) := \text{sgn}(\boldsymbol{\Gamma})$$

Here we're just repurposing the notation $\boldsymbol{\Gamma}$ to indicate the vector which gets thresholded to -1 and $+1$ by the sign function to generate the new state $\hat{\mathbf{x}}^{(2)}[1]$. Some of the components of the vector $\hat{\boldsymbol{\delta}}^{(2)}[1] \odot \mathbf{c}$ will be the same as $\mathbf{x}_\star^{(2)}$ and some (hopefully small) number of the components will have been flipped compared to $\mathbf{x}_\star^{(2)}$ by the update to factor 1. Let us denote the set of components which flipped as \mathbb{Q} . The set of components that did not flip is \mathbb{Q}^c . The number of bits that did or did not flip is the *size* of these sets, denoted by $|\mathbb{Q}|$ and $|\mathbb{Q}^c|$, respectively. We have to keep track of these two sets separately because it will affect the probability that a component of $\hat{\mathbf{x}}^{(2)}[1]$ is flipped relative to $\mathbf{x}_\star^{(2)}$. We can write out the constant and random parts of Γ_i along the same lines as what we did in (45).

$$\begin{aligned} \Gamma_i &= \sum_m^{M_2} \sum_j^N (\mathbf{x}_m^{(2)})_i (\mathbf{x}_m^{(2)})_j (\hat{\boldsymbol{\delta}}^{(2)}[1] \odot \mathbf{c})_j \\ &= \sum_m^{M_2} \sum_{j \in \mathbb{Q}^c}^N (\mathbf{x}_m^{(2)})_i (\mathbf{x}_m^{(2)})_j (\mathbf{x}_\star^{(2)})_j - \sum_m^{M_2} \sum_{j \in \mathbb{Q}}^N (\mathbf{x}_m^{(2)})_i (\mathbf{x}_m^{(2)})_j (\mathbf{x}_\star^{(2)})_j \\ &= |\mathbb{Q}^c| (\mathbf{x}_\star^{(2)})_i + \sum_{m \neq \star}^{M_2} \sum_{j \in \mathbb{Q}^c}^N (\mathbf{x}_m^{(2)})_i (\mathbf{x}_m^{(2)})_j (\mathbf{x}_\star^{(2)})_j - |\mathbb{Q}| (\mathbf{x}_\star^{(2)})_i - \sum_{m \neq \star}^{M_2} \sum_{j \in \mathbb{Q}}^N (\mathbf{x}_m^{(2)})_i (\mathbf{x}_m^{(2)})_j (\mathbf{x}_\star^{(2)})_j \\ &= (N - 2|\mathbb{Q}|) (\mathbf{x}_\star^{(2)})_i + \sum_{m \neq \star}^{M_2} \sum_{j \in \mathbb{Q}^c}^N (\mathbf{x}_m^{(2)})_i (\mathbf{x}_m^{(2)})_j (\mathbf{x}_\star^{(2)})_j - \sum_{m \neq \star}^{M_2} \sum_{j \in \mathbb{Q}}^N (\mathbf{x}_m^{(2)})_i (\mathbf{x}_m^{(2)})_j (\mathbf{x}_\star^{(2)})_j \quad (47) \end{aligned}$$

If i is in the set of bits which did not flip previously, then there is a constant $(M_2 - 1)(\mathbf{x}_\star^{(2)})_i$ which comes out of the second term above. If i is in the set of bits which did flip previously, then there is a constant $-(M_2 - 1)(\mathbf{x}_\star^{(2)})_i$ which comes out of the third term above. The remaining contribution to Γ_i is, in either case, a sum of $(N - 1)(M_2 - 1)$ i.i.d. Rademacher random variables, analogously to what we had in (45). Technically $|\mathbb{Q}|$ is a random variable but when N is of any moderate size it will be close to $r_1 N$, the bitflip probability for the first factor. Therefore, Γ_i is approximately Gaussian with mean either $(N(1 - 2r_1) + (M_2 - 1))(\mathbf{x}_\star^{(2)})_i$ or $(N(1 - 2r_1) - (M_2 - 1))(\mathbf{x}_\star^{(2)})_i$, depending on whether $i \in \mathbb{Q}^c$ or $i \in \mathbb{Q}$. We call the *conditional* bitflip probabilities that result from these two cases $r_{2'}$ and $r_{2''}$:

$$\begin{aligned} r_{2'} &:= Pr\left[(\hat{\mathbf{x}}^{(2)}[1])_i \neq (\mathbf{x}_\star^{(2)})_i \mid (\hat{\boldsymbol{\delta}}^{(2)}[1] \odot \mathbf{c})_i = (\mathbf{x}_\star^{(2)})_i\right] \\ &= \Phi\left(\frac{-N(1 - 2r_1) - (M_2 - 1)}{\sqrt{(M_2 - 1)(N - 1)}}\right) \quad (48) \end{aligned}$$

$$\begin{aligned} r_{2''} &:= Pr\left[(\hat{\mathbf{x}}^{(2)}[1])_i \neq (\mathbf{x}_\star^{(2)})_i \mid (\hat{\boldsymbol{\delta}}^{(2)}[1] \odot \mathbf{c})_i \neq (\mathbf{x}_\star^{(2)})_i\right] \\ &= \Phi\left(\frac{-N(1 - 2r_1) + (M_2 - 1)}{\sqrt{(M_2 - 1)(N - 1)}}\right) \quad (49) \end{aligned}$$

G.3 All other factors

It hopefully should be clear that the general development above for the bitflip probability of the second factor will apply to all subsequent factors – we just need to make one modification to notation. What really determines whether a component of $\hat{\mathbf{o}}^{(f)}[1] \odot \mathbf{c}$ equals the corresponding component of $\mathbf{x}_\star^{(f)}$ is the *net* bitflip seen by the f th factor. It might be the case that the component had initially flipped but was flipped back by subsequent factors – all that matters is whether an *odd* number of previous factors flipped the component. We define the quantity n_f to be the net bitflip probability that is passed on to down-stream factors:

$$n_f := Pr[(\hat{\mathbf{o}}^{(f+1)}[t] \odot \mathbf{c})_i \neq (\mathbf{x}_\star^{(f+1)})_i] \quad (50)$$

For the first factor, $r_1 = n_1$ but in the general case it should be clear that

$$r_f = r_{f'}(1 - n_{f-1}) + r_{f''}n_{f-1} \quad (51)$$

Which is just marginalizing over the probability that a net bitflip was not seen (first term) and the probability that a net bit was seen (second term). The expression for the general n_f is slightly different.

$$n_f = r_{f'}(1 - n_{f-1}) + (1 - r_{f''})n_{f-1} \quad (52)$$

In (48) and (49) above we had r_1 but what really belongs there in the general case is n_1 . This brings us to our general statement for the conditional bitflip probabilities $r_{f'}$ and $r_{f''}$:

$$r_{f'} = \Phi\left(\frac{-N(1 - 2n_{f-1}) - (M_f - 1)}{\sqrt{(M_f - 1)(N - 1)}}\right) \quad (53)$$

$$r_{f''} = \Phi\left(\frac{-N(1 - 2n_{f-1}) + (M_f - 1)}{\sqrt{(M_f - 1)(N - 1)}}\right) \quad (54)$$

What we have derived in this appendix are the equations (19) and (20) - (27) from the main text. Clearly the bitflip probability for a Resonating Circuit differs from a Hopfield Network due to percolated noise between the factors – we demonstrate by how much it differs in Section 4.1.